Journal of Quantitative Spectroscopy & Radiative Transfer 324 (2024) 109055

Contents lists available at ScienceDirect

Journal of Quantitative Spectroscopy and Radiative Transfer

journal homepage: www.elsevier.com/locate/jqsrt

The pressure dependence of the experimentally-determined line intensity and continuum absorption of pure CO_2 in the 1.6μm region

M. Birk *, C. Röske, G. Wagner

Remote Sensing Technology Institute, German Aerospace Center (DLR), Wessling D-82234, Germany

ARTICLE INFO

Keywords:
Carbon dioxide
Pressure-dependent line intensity
Continuum
High accuracy Fourier transform measurements
atmospheric CO2 measurements

ABSTRACT

Fourier-transform measurements of pure CO_2 spectra in the 1.6 μm region covering bands from the ground state to the 30011, 30012, 30013, and 30014 states at ambient temperature and 212 K with pressures up to 1 atm have been recorded. The measured spectra have been multispectrum-fitted with the Hartmann-Tran model with first order line-mixing taken into account. In the fits, a linear decrease of the line intensities with increasing pressure was introduced. From the fitted baselines, the self-continuum, which complements the contribution of the local lines within +/− 25 cm^{-1}, was determined for the two strongest bands, 30012–00001 and 30013–00001. The depleted intensity was found to be transferred to the continuum for both temperatures. The intensity in the continuum at 1 atm was about 1 % of the total band intensity for ambient temperature and about 3 % at 212 K. For both temperatures, the average depleted intensity/continuum area was found in excellent agreement with values estimated from the second virial coefficient. From these results, a new spectroscopic database with pure CO_2 line profile parameters was produced, with systematic line intensity uncertainties well below 0.1 %.

Retrieval simulations for the CO_2 1.6 μm and 2 μm bands measurements, planned with the future CO2M mission, similar to the OCO mission, were carried out to assess the impact of intensity depletion and continuum. The impact of the continuum was larger than that of the depletion and larger for the 2 μm band than for the 1.6 μm band, with a substantial column error of 2 % for the 2 μm band when omitting both, depletion and continuum.

The findings regarding pressure-dependent intensity and continuum may be applicable to other in-band continua showing similarity to the monomer band in shape and position. The new results may increase the knowledge on the physical nature of continua.

1. Introduction

So far, radiative transfer models and most fits and analyses of laboratory spectra assume the line intensity feeding the modelled line shape to be independent of pressure. However, it was shown a while ago for some hydrogen halide gases that the integrated line intensities retrieved from fits of isolated lines in measured spectra may decrease with increasing total pressure, specifically up to 1 %/bar for HCl in Ar [11] and 2 %/bar for HF in Xe [22]. These findings were recently confirmed by Tran et al. [37,38] who pointed out decreases of up to 3 %/bar for pure HCl, of up to 3 %/bar and 0.8 %/bar for HCl broadened by CO_2 and air, respectively, while no effect was observed for HCl diluted in He. It was experimentally demonstrated that for these systems, the effect decreases with the line rotational quantum number. It is only very recently that this issue was investigated for a more "common" molecule by Reed at al. [28] who pointed out similar, but smaller effects for CO in nitrogen, confirming a previously observed influence of the rotational quantum number, and the negligibility of effects in CO-He mixtures. The observed decreases of the retrieved line intensity with pressure was attributed to the non-Markovian behavior of collisions or the breakdown of the impact theory [23,28,36–38] and/or to the formation of gaseous molecular complexes [22,41]. In [28,37,38], using re-quantized classical molecular dynamics simulations (rCMDS), absorption spectra of HCl and CO with various collision-partners were computed. It was shown that the pressure dependences of the line intensity determined from the simulated spectra are in good agreement with experimental values. Analysis of the time evolution of the molecular populations for different rotational levels, computed by rCMDS, showed that the pressure dependence of the line intensity determined from fits of measured or calculated spectra using a usual impact line-shape model [26] and

* Corresponding author.
E-mail address: manfred.birk@dlr.de (M. Birk).

https://doi.org/10.1016/j.jqsrt.2024.109055
Received 18 January 2024; Received in revised form 16 May 2024; Accepted 17 May 2024
Available online 22 May 2024
0022-4073/© 2024 The Authors. Published by Elsevier Ltd. This is an open access article under the CC BY license (http://creativecommons.org/licenses/by/4.0/).

references therein] is due to the effects of non-Markovian collisions, which are neglected in the impact approximation.

Before pressure dependent intensities were considered, line intensities with about 0.1 % accuracy were claimed by few authors [5,8,9,18,24] for CO and CO_2. Some of these studies have been motivated by the remote sensing of greenhouse gases, which imposes demanding requirements on the accuracy of spectroscopic data. For instance, the requirement for absolute line intensity accuracies for CO_2 is better than 0.2 % [21]. In addition, improving the accuracy is of metrological interest and of importance for comparison with theoretical calculations [5]. Certainly, all of these results have to be reconsidered in the light of the pressure dependence of experimentally-determined intensity.

During the analysis of ambient temperature air-broadened CO_2 spectra in the 1.6 μm region within the ESA-funded ISOGG project [21], pressure-dependent intensity was discovered, but due to the gas mixing and wall sticking issues of CO_2/air the results were deemed not conclusive. In order to avoid such problems associated with gas mixtures, pure CO_2 measurements up to 1000 mbar were conducted at 294 K and 212 K which are described in this paper. The analyses of the spectra were made applying a multispectrum fitting approach with the Hartmann-Tran profile (HTP) [26]. This enabled the determination of the spectroscopic line parameters, and a decrease of the retrieved line intensity with pressure along with its rotational dependence, as well as the continuum.

In the present work, the pressure-dependence of intensity was found to be linked to the continuum. The understanding of continua is still not complete (see, for example, a historical review on water continua [33] and references therein). For the water in-band self-continuum, Serov et al. [32] suggest that the real gas pressure correction expressed in terms of the virial coefficients is linked to the existence of dimers. Thus, the decrease of pressure with respect to an ideal gas is fully explained by dimer formation. The continuum is thought to be a combination of bound and quasi-bound dimer absorption. However, the sum of both dimers exceeds the number expected from the second virial coefficient [7,27]. Serov et al. also suggested a contribution from super-Lorentzian line wings of the monomer, which are thought not to contribute to the second virial coefficient.

Although experimental CO_2 self-continua, to our knowledge, are not available so far, there are results on CIA in symmetry-forbidden bands $\nu_2+\nu_3$ [4], $2(\nu_1/2\nu_2)$ [3], and $\nu_1/2\nu_2$ [40]. The CIA data is available in HITRAN2020 [19]. These CIA bands are based on bimolecular absorptions and structures of the CO_2 dimer, appearing in the $\nu_1/2\nu_2$ and 2 $(\nu_1/2\nu_2)$ bands but not in the $\nu_2+\nu_3$ band. In case of the $\nu_1/2\nu_2$ band theoretical calculations confirm the experimental results. These calculations are based on [39] who derived a rigorous treatment of bimolecular absorptions. Using special conditions for energy-related quantities he differentiated between bound dimers, quasi-bound dimers, and free pairs.

The remainder of this paper is divided into seven sections. First, the experiment and the analysis are described. Then, details of the new results regarding the pressure dependence of line intensity, the continuum, and second virial coefficient are given. In the following section retrieval simulations aress described, investigating the impact of depletion and continuum on CO_2 retrieval of simulated observations with a CO2M type satellite instrument. Then, these results on intensity depletion, continuum and their connection to the second virial coefficient are discussed and line intensities and self-broadening parameters are compared to previous work. The next section describes the new spectroscopic database. In the conclusion, results are summarized and the impacts of the results for spectroscopic databases, future laboratory measurements, and remote sensing are detailed.

2. Experiment

Since the experimental details are close to those of [8], only the improvements made since this previous study are mentioned here. It turned out that during the measurements of [8] a problem of the position readout of the scanning interferometer mirror of the Bruker IFS 125HR was present, causing offsets in the permille range. This was repaired before the conduction of measurements reported in this work. A commercial optical 1.5 μm high-pass filter was implemented, limiting the upper bound of the spectral range to ca. 6850 cm^{-1} and thus improving the signal-to-noise ratio by a factor 1.5. The lower limit of 5800 cm^{-1} is still determined by the InGaAs detector. The spectral range covers the four bands 30011, 30012, 30013, and 30014 (upper state labels in the HITRAN database convention, lower states being the ground state). The accuracy of the multireflection cell absorption path determination was improved from 0.1 % to 0.02 % by caliper measurements of the T-mirror – D-mirror distance in combination with raytracing. In addition, the cell mirrors' coatings were changed from gold with a reflectance of 0.985 at 6200 cm^{-1}, to a dielectric coating with a reflectance of 0.999 below 6400 cm^{-1}. This significantly improved the signal-to-noise ratio, especially for long absorption paths which involve many reflections: e.g.: factors of 1.3 and 2.9 for 14 m and 117 m, respectively. Finally, a more accurate pressure sensor was purchased (Mensor CPG2500 with sensor CPR2550, range 1000 mbar, accuracy 0.008 % above 300 mbar).

As in ref. [8], pure CO_2 (Linde company, purity 0.99995, further purification to 0.999995, $^{12}CO_2$ abundance given in HITRAN is assumed) was filled into the cell and for all measurements with pressures of 75 mbar and above the spectra were recorded while the cell was sealed off, while a steady flow was used at 10 and 30 mbar to avoid non-negligible pressure contributions due to accumulated leakage and outgassing. All measurements together with the relevant conditions for ambient temperature are summarized in Table 1 and those for 212 K are given in Table 2. Since self-continua underlying the contribution of local lines have a quadratic pressure dependence, the relative pressure increments were decreased towards higher pressures. The measurements at the lowest pressure, at 10 mbar, were used for instrumental line shape (ILS) determination and thus required a considerably better signal-to-noise ratio, which was achieved by a longer measurement time (see Tables 1 and 2). The absorption path of 14 m was selected for most

Table 1
Ambient temperature CO_2 measurement conditions. p_{CO2}: measured pressure, $F_{n\text{-}corr}$: number density correction factor, l: absorption path, T: gas temperature, t_{meas}: measurement time. Recording time of a single interferogram is 81 s. SNR_{RMS} gives the root mean square signal-to-noise ratio (the inverse noise level at 100 % transmittance) at 6400 cm^{-1}. The SNR varies by less than 10 % over the region (6020–6575 cm^{-1}). Combined standard uncertainties are given between parentheses in units of the last digit. For the 117 m absorption path measurements, serving only for offset determination, the pressure correction could be ignored.

Meas.	p_{CO2} (mbar)	$F_{n\text{-}corr}$	l (cm)	T (K)	t_{meas} (min)	SNR_{RMS}
#1	10.0002 (62)	1.0000	1456.40 (29)	294.23 (10)	880	14,000
#2	30.115 (20)	1.0001	1456.40 (29)	294.23 (10)	82	4700
#3	75.227 (24)	1.0004	1456.40 (29)	294.23 (10)	82	4900
#4	151.443 (24)	1.0008	1456.40 (29)	294.22 (10)	82	5000
#5	298.696 (24)	1.0015	1456.40 (29)	294.22 (10)	82	4800
#6	503.693 (40)	1.0026	1456.40 (29)	294.23 (10)	82	4900
#7	749.742 (60)	1.0039	1456.40 (29)	294.23 (10)	82	4900
#8	982.351 (79)	1.0051	1456.40 (29)	294.23 (10)	82	4900
#9	10.0052 (62)		11,695.92 (98)	294.23 (10)	1017	14,000
#10	100.721 (24)		11,695.92 (98)	294.23 (10)	82	4000

Table 2
212 K CO_2 measurement conditions. Symbols see Table 1. T_{fit} is the gas temperature fitted from relative line intensities. Inhom is defined as T_{fit}=*Inhom**294K+(1-*Inhom*)*212 K (see Section 3.1.6). SNR_{RMS} gives the root mean square signal-to-noise ratio (the inverse noise level at 100 % transmittance) at 6400 cm^{-1}. The SNR varies by less than 10 % over the region (6020–6575 cm^{-1}). Combined standard uncertainties are given in parentheses in units of the last digit.

Meas.	p_{CO2} (mbar)	$F_{n\text{-}corr}$	l (cm)	T (K)	T_{fit} (K)	*Inhom* (%)	t_{meas} (min)	SNR_{RMS}
#11	9.9989(62)	1.0000	1456.33 (29)	210.25(10)	210.03(10)	0	880	15,000
#12	518.928(42)	1.0072	1456.33 (29)	210.26(10)	211.75(30)	2.1	54	3800
#13	749.619(60)	1.0104	1456.33 (29)	209.99(10)	212.36(30)	3.2	54	4000
#14	998.961(80)	1.0138	1456.33 (29)	210.32(10)	212.95(30)	3.6	54	3800

measurements, at 10 mbar the intensity of the lines is below 35 % absorption while for 1000 mbar it is below 90 %. The rms noise on the transmittance baseline in a region free of lines is typically around 1/5000 (or 2×10^{-4}) for ambient and around 1/4000 for low temperature. Thus, for the strongest lines, the peak-to-peak noise amplitude is about 0.1 % of the peak line intensity. In order to detect and quantify an eventual instrumental offset affecting the measured 0 % transmittance, measurements were recorded at an absorption path of 117 m and a pressure of 100 mbar. For 100 mbar, the strongest lines have optical depths >15, corresponding to a transmittance $<3 \times 10^{-7}$, which is well suited for determining the 0 % transmittance level. An additional 10 mbar measurement serves for ILS determination.

Number densities calculated from the measured pressures using the ideal gas law have to be corrected for real gas effects. The impact of this correction is twofold. First, intensities are linked to number densities. Second, the collisional parameters (pressure-broadening and -shifting, line-mixing parameters, frequency of velocity-changing interactions) in the line profile (see below) are proportional to the number densities. At room temperature, corrections were calculated using the NIST tool REFPROP [courtesy Joseph T. Hodges, NIST]. The correction is +0.5 % at 980 mbar. Alternatively, the calculations were performed according to the Soave-Redlich-Kwong (SRK) equation of state [34] applying the critical pressure, temperature, and the acentric factor [2] leading to excellent agreement with NIST results. At low temperature (212 K), for which no NIST data are available, the Soave-Redlich-Kwong equation of state was applied with a significantly larger correction of +1.4 % at 1000 mbar. The resulting correction differences between ambient temperature NIST and Soave-Redlich-Kwong corrections are well below the pressure uncertainty, thus the relative pressure sensor uncertainty given in the first column of Tables 1 and 2 should be used as the uncertainty of the corrected number density. Outgassing and leakage could be neglected.

For the ambient temperature spectra, the temperature sensor readings were used for the analysis, while for the low temperature ones, the mean gas temperature was determined from the retrieved line intensities, using ambient temperature line intensities as a reference (see Analysis section). Furthermore, the inhomogeneity is given in Table 2 (see Analysis section for definition).

Gas sample interferograms were recorded with a maximum optical path difference of 100 cm, corresponding to a resolution of 0.005 cm^{-1}, as in [8]. The empty cell measurements were obtained with a maximum optical path difference of 1.8 cm and conducted mostly before and after the measurements with the gas samples. The transmittance spectra were then obtained by dividing the sample by the reference spectra after selecting a single or a combination of reference spectra, in order to minimize the etalon-type fringes.

3. Analysis

For the analysis of the spectra, the multispectrum fitting tool described in [8] and references therein was applied. This enables to retrieve a set of individual line parameters together with the continuum, which is derived applying the method described in [7]. The advantage of this method is that all these quantities are obtained from the same spectra, so that the imperfections of the individual line-shape model appear in the continuum and the broadband residuals of the fit of measured spectra contain mostly noise. Thus, using the database (line parameters+continuum) provided in this paper ensures the best quality of retrievals from remote sensing spectra. This contrasts with the common approach, e.g. for water vapor, which uses a spectroscopic database like HITRAN [19] together with the MT_CKD continuum [25], where the spectroscopic line parameters and the continua originate from different sources, which may introduce biases in the simulations.

3.1. Analysis of experimental spectra

3.1.1. Instrumental line shape

The instrumental line shape (ILS) determination is described in detail in [8]. The impact of the ILS is smaller in the present work because here, pressures range from 10 to 980 mbar instead of from 10 to 80 mbar, while the width of the ILS is the same. Since the instrument as well as the techniques to achieve a stable and reproducible ILS were improved, the errors associated with the assumed ILS should be smaller. The 10 mbar and 30 mbar pure CO_2 measurements (#1, #2, #11 in Tables 1 and 2) were used for ILS determination. During the analysis of CO spectra [9], a small low resolution (3 cm^{-1} wide) ILS contribution was discovered when coadding residuals of the multispectrum fitting. This contribution is only discernible from the noise at higher pressures where the line area is larger. The LINEFIT software [20] used for the ILS determination only considers higher resolution line shape information. The low-resolution line shape contribution was calculated from co-added residuals and was implemented in the multispectrum fitting. The residuals were slightly improved but the impact on most line parameters was found to be negligible. The final results given in this paper were obtained using the 10 mbar ILS because the information content of the narrower lines in the 10 mbar measurement for the ILS determination is higher. For the low temperature spectra, the impact of the ILS was negligible since all sample pressures are above 500 mbar. The 10 mbar low temperature measurement, dedicated to the analysis of the low temperature measurements, was thus not needed for ILS determination, but was used for line intensity validation.

3.1.2. 0 % level

An intensity offset affecting the 0 % transmittance level (i.e. total saturation) in the measured spectra would yield an error in the retrieved line parameters and, to much smaller extent, the continuum. Usually such an offset is linked to a detector non-linearity [6] but it turned out that it can also result from errors of the optical path difference measurements in the interferogram. Such sampling errors might have been present in the instrument during the measurements of Ref. [8], but they were not obvious at that time. Later-on, but before the measurements for the present work, offsets in the range of 0.2 % in transmittance were clearly observed and attributed to a hardware error which was fixed. In order to assess possible offsets in the present measurements, the spectra #9 and #10 were recorded and analyzed with the multispectrum fitting tool. The offset was fitted as a parameter in the multispectrum fitting for microwindows containing the strongest lines and was averaged. A non-zero offset of −0.046(3)% in transmittance was still present. All spectra were corrected accordingly.

3.1.3. Line parameter retrieval from ambient temperature measurements

In order to retrieve the line parameters and continuum, only measurements #2-#8 were considered in the multispectrum fit. Measurement #1 was previously used for the ILS determination (see above) and, later on, is used for the validation of the line intensities. Automatically chosen 7 to 16 cm^{-1} wide adjacent microwindows, with limits between absorption lines, were treated sequentially in the region 5970–6575 cm^{-1}. The microwindows should not be smaller, since then line mixing could be fitted as baseline, resulting in wrong baseline and line mixing parameters (see [7]). All lines contributions were cut at ±25 cm^{-1} from the transition center. A line shape was applied assuming a Quadratic Speed-Dependent Hard Collision model including line-mixing (LM) through the 1st order approximation [29], i.e. a Hartmann-Tran profile [26] with LM and no correlation (η=0). The contributions from lines which are not further away from the borders of the microwindow than 25 cm^{-1} are included in the spectrum calculation. From the 27,000 lines within the region of interest listed in the HITRAN2020 database [19] 1200 were considered to be "fittable". Lines which were too weak or highly blended by strong lines were not considered as "fittable". For fittable weak lines only the line position, σ_0, and intensity, S, were fitted. With increasing line intensity S (expressed hereafter in units of $cm^{-1}cm^2molecule^{-1}$), the self-broadening, $\gamma_{0,self}$ (for $S > 5 \times 10^{-27}$), self-shift, $\delta_{0,self}$ (for $S > 5 \times 10^{-27}$), speed dependence of self-broadening, $\gamma_{2,self}$ (for $S > 1.5 \times 10^{-25}$), and for the stronger lines, the 1st order line mixing coefficient, Y_{self} (for $S > 1.5 \times 10^{-25}$), the speed dependence of self-shift, $\delta_{2,self}$ (for $S > 2 \times 10^{-24}$), and the frequency of velocity changes, $\nu_{VC,self}$ (for $S > 3 \times 10^{-24}$) were fitted. Parameters which are not fittable and which are standard parameters of the HITRAN database (σ_0, S, $\gamma_{0,self}$) are taken from HITRAN2020. $\delta_{0,self}$, Y_{self}, $\delta_{2,self}$, and $\nu_{VC,self}$ are set to zero. $\gamma_{2,self}$ is set to a polynomial value (see Section 4. Line parameter retrieval in [8]). For each line, an intensity correction parameter, labeled d_{self}, was introduced such that $S(p)$=$S(p = 0) \times [1+d_{self} \times p(\text{atm})]$. The product $d_{self} \times p(\text{atm})$ is called "pressure-dependent intensity correction fraction" (PDIC) in the following. Alternatively, the phrase "depleted intensity" is used. This linearity of line intensities with pressure, previously shown for other systems in, e.g. [28,37,38], is demonstrated in Fig. 10 in Section "Intensity correction, continuum, and second virial coefficient". d_{self} was fitted for lines with $S > 5 \times 10^{-25}$. For fittable but weaker lines, d_{self} was set to zero, and for following iterations it was set to the average of the intensity-weighted averaged values of the 30012 and 30013 bands. A quadratic baseline polynomial was fitted in each microwindow. A 3rd order polynomial was also tested but did not have a significant impact on the fitted line parameters. After a first fitting round, the retrieved unperturbed line positions were compared with those from [8] and a calibration factor (no offset) was determined. The calibration factor was then used in the multispectrum fit to ensure that unfitted lines are calibrated correctly. It turned out that small non-reproducibilities in the instrumental line shape between different measurements caused systematic residuals for measurements #3, #4, and #5. For the latter, individual calibration factors for each microwindow were fitted in the multispectrum fit. It should be noted that the line position is the most sensitive indicator for the ILS reproducibility, even without noticeable impact on the line profile, especially at higher pressures. The second fitting round enables to improve the retrieved quantities, since the contributions of lines outside the currently treated microwindow are computed using parameters obtained from the first round (while they were fixed to a priori chosen values in the first fit, see above). After this procedure, the obtained parameters were inspected for precision and whether they were in a physically reasonable range. In a third fitting round, those parameters with unrealistic values or too large uncertainties were removed from the fit and set to the defaults (see above). Furthermore, residuals were inspected and, when exceeding twice the peak-to-peak noise, the selection of fitted line parameters was altered manually for improvement. An example screenshot for a final fit of a microwindow is shown in Fig. 1, showing that the residuals are essentially noise, but some residuals are also visible, on the order of 0.06 % of the peak absorption. The goodness of fit, χ, of the multispectrum fitting for all microwindows are smaller than 1.1, most of them being around 1. χ is given by the sqrt (average of (observed-calculated)$^2/\sigma^2$), where σ is the a priori statistical

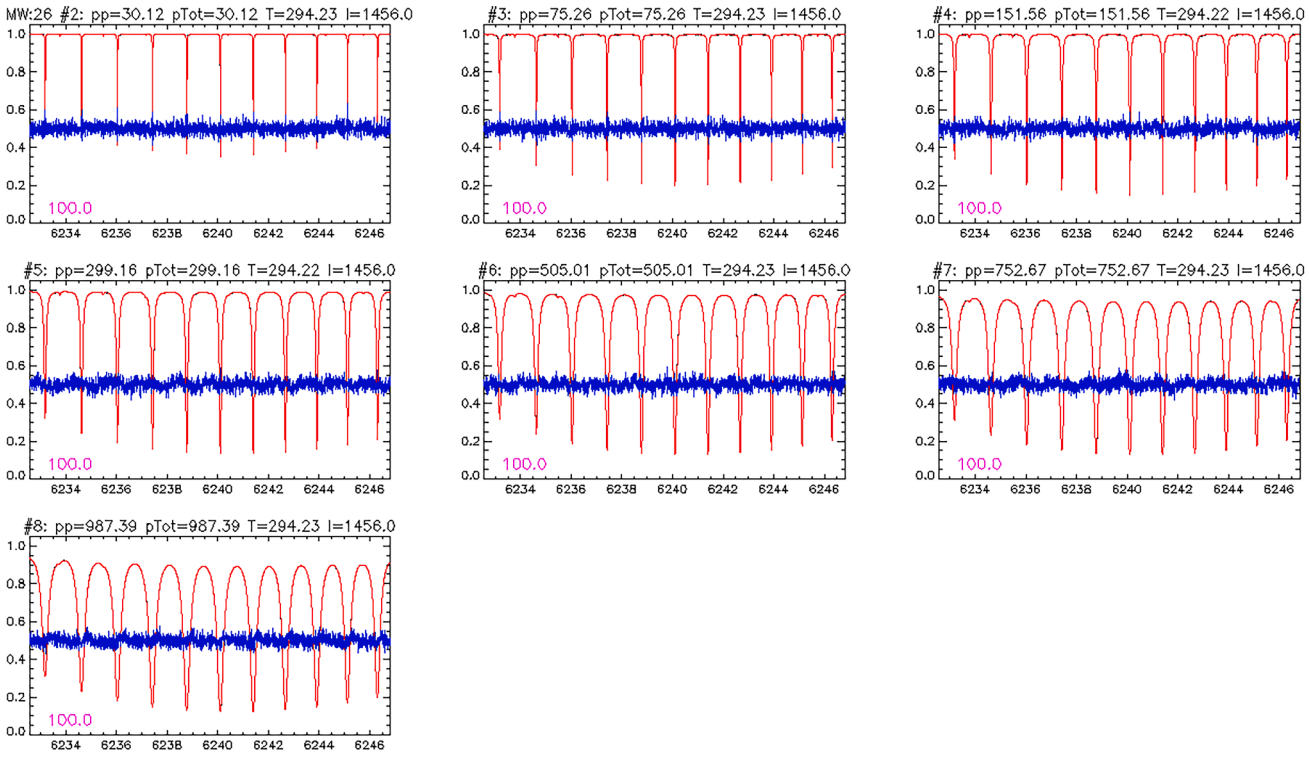

Fig. 1. Example screenshot of multispectrum fit of measured transmittance spectra, for the R6 to R26 lines of the 30013 band and various pressures. The residuals, in blue, have been multiplied by 100. The numbering of spectra corresponds to Table 1.

uncertainty, i.e. the rms noise in this case. The largest non-noise residuals in the entire spectral range occur for the strongest lines in the R-branches of the 30012 and 30013 bands (Fig. 1) for spectra with pressures of 300 mbar and above.

3.1.4. Line parameter retrieval from low temperature measurements

The low temperature measurements #2 (527 mbar), #3 (757 mbar), and #4 (1013 mbar) (Table 2) were analyzed with the multispectrum fitting software keeping the ambient temperature parameters fixed to the results from Section 3.1.3. The following parameters were fitted: temperature exponent of $\gamma_{0,self}$, n_{self} ($S > 2 \times 10^{-26}$), temperature exponent of $\gamma_{2,self}$, $n_{\gamma 2,self}$ ($S > 10^{-24}$), temperature dependence of pressure-induced line shift, $T\delta_{0,self}$ ($S > 10^{-25}$), line mixing at 212 K, $Y_{self,212\ K}$ ($S > 10^{-25}$), intensity correction parameter at 212 K, $d_{self,212\ K}$ ($S > 10^{-25}$), line intensity limits refer to 212 K. A single wavenumber calibration factor common to all measurements was fitted. For line mixing we first implemented a temperature exponent, but for situations where the sign of the line mixing changes with temperature (close to the intensity maxima of the individual branches), this approach fails. Therefore, we fitted an independent line mixing parameter at 212 K. Since d_{self} is a new parameter and there is nothing known about its temperature dependence, we fitted independent d_{self} at 212 K. For $T\delta_{0,self}$ (in $cm^{-1}atm^{-1}K^{-1}$) we used the following definition: $\delta_{0,self}(T)=\delta_{0,self}(296\ K)+T\delta_{0,self} \times (T-296\ K)$. With the temperature dependence parameters fixed, the ambient temperature measurements were refitted since the measurement temperature was 2 K below the reference temperature (296 K).

3.1.5. Line parameter uncertainties from ambient temperature measurements

The uncertainty estimation is described in detail in [8]. In the line parameter database for S, $\gamma_{0,self}$, $\gamma_{2,self}$, d_{self}, provided in the present study, two uncertainties are given: The statistical ones (type A) from the multispectrum fit and systematic uncertainties (type B). The temperature-induced line intensity uncertainties (type B) are also given. For all the other line parameters, only the statistical uncertainties are tabulated in the line parameter database. All zero-pressure line intensity related systematic error sources along with their associated uncertainties in the present work are summarized in Table 3.

The ILS-induced uncertainty was obtained from a multispectrum fitting with the ILS derived from the 30 mbar measurement by comparing the associated retrieved parameters with those derived with the 10 mbar ILS. It should be emphasized that this is only an estimate since the individual ILS for each measurement is unknown. On the other hand, the influence of an ILS-induced error decreases with pressure and, from our experience with the ILS stability and reproducibility, we know that the results here are reasonable.

The following ILS-induced uncertainties were found: S 0.05 %, $\gamma_{0,self}$ 0.07 %, $\gamma_{2,self}$ 1 %, d_{self} 8 %, Y_{self} 4×10^{-5} atm^{-1} (negligible compared with statistical uncertainty), $\nu_{VC,self}$ 15 %, $\delta_{0,self}$ 2×10^{-6} cm^{-1}/atm, $\delta_{2,self}$ negligible.

The pressure uncertainties listed in Table 1 were propagated into the zero pressure line intensity S (0.02 %) and the intensity correction parameter d_{self} (1 %) uncertainty. Otherwise, the pressure-induced systematic uncertainties are only relevant for $\gamma_{0,self}$ and are about 0.01 %.

Regarding line profile errors for the lines for which less parameters were fitted, zero pressure line intensities show a negligible impact when omitting $\nu_{VC,self}$ and $\delta_{2,self}$, but the impact on $\gamma_{0,self}$ was about 0.05 %.

Systematic line position uncertainties were determined from the average line difference between those of the present work and [8], leading to a value of 1.7×10^{-6} cm^{-1}.

In order to assess the impact of a temperature error, the multispectrum fit was carried out, increasing all experimental temperatures by 0.1 K, as done in [8]. For the intensities the effect depends on the lower state energy and ranges from +0.08 % at 0 cm^{-1} lower state energy to −0.25 % at 1800 cm^{-1}. For the other line parameters, the impact is negligible.

For σ_0 and $\delta_{0,self}$, where the systematic uncertainty was defined as an offset and it is thus identical for all lines, no entries in the database are given.

The quality of the determination of the zero pressure line intensities and the associated values of d_{self} can be assessed by a number density factor fit [8]. For that, the spectroscopic parameters are fixed to the results of the multispectrum fitting and, for each microwindow and each spectrum, number density and wavenumber calibration factors are fitted. The number density factors (*NDfactors*) are factors the inputted number densities are multiplied with in the fitting procedure to minimize residuals. The microwindow width for this purpose was 3–4 cm^{-1}. The resulting number density factors vs. line intensity are displayed in Fig. 2, and the average *NDfactors* are summarized in Table 4. The line intensity in each panel of Fig. 2 refers to the most intense line in the corresponding microwindow. Only microwindows containing lines with $S > 5 \times 10^{-25}$ $cm^{-1}cm^2molecule^{-1}$ are considered because the depletion fit is limited to those lines. The average *NDfactors* all differ from 1 by less than 0.1 % and less than 0.01 % for pressures ≥150 mbar. There is only a very small intensity dependence of the *NDfactors*, an ultrahigh quality that had not been reached in [8] due to the experimental improvements described in Section 2 and the introduction of the depletion parameter. The largest systematic deviation of 0.08 % occurs for the 10 mbar measurement, which is close to the accuracy of the pressure sensor (0.06 %). The results show that the pressure errors including the real gas number density correction are within the specification given in Table 1. The *NDfactor* analysis also shows the absence of opacity-dependent and line width-dependent errors. Thus, the line shape model and ILS are excellent. These good results are also related to the low largest optical depth of 2.1, in contrast to 6.5 in [8]. Due to the exponential dependence of the transmittance on the optical depth, the impact of several systematic errors increases with optical depth.

3.1.6. Line parameter uncertainties from low temperature measurements

The main systematic uncertainties on the parameters retrieved from 212 K spectra arise from the temperature inhomogeneities in the cell, and they are significant for the temperature exponent $n_{\gamma 0,self}$ and for the intensity correction parameter d_{self}. The reason for the temperature inhomogeneity is that the flanges of the multireflection cell are at ambient temperature. The flanges are outside the IR path but convection transports some warm gas into the space between the mirrors. To quantify the temperature inhomogeneity we defined an inhomogeneity parameter, *Inhom*: $Tfit=Inhom \times 294\ K+(1-Inhom) \times 212\ K$, where 212 K is the measured cell/mirror temperature, and *Tfit* is the gas temperature fitted from the measured line intensities (see Table 2). While at 10 mbar without convection the inhomogeneity parameter is zero, it is largest for the highest pressure, where convection is largest and 3.6 % of the molecules are at ambient temperature and 96.4 % are at 212 K (see Table 2). In the estimate of systematic errors for temperature exponent and depletion, the temperature dependence of the line intensity was ignored, i.e. the intensity contributions of the 212 K and the 294 K regions are only proportional to the percentage of gas at the respective temperature. The error propagation yields that the temperature

Table 3
Summary of systematic zero pressure line intensity error sources and associated uncertainties. Molecular line shape uncertainties refer to the impact of not fitting parameters in the line profile.

Physical Effect	Uncertainty/%
Systematic uncertainty in ILS	0.05
Pathlength	0.02
Molecular line shape	Negligible
Pressure (drives density and depletion)	0.02
Root sum square	0.06

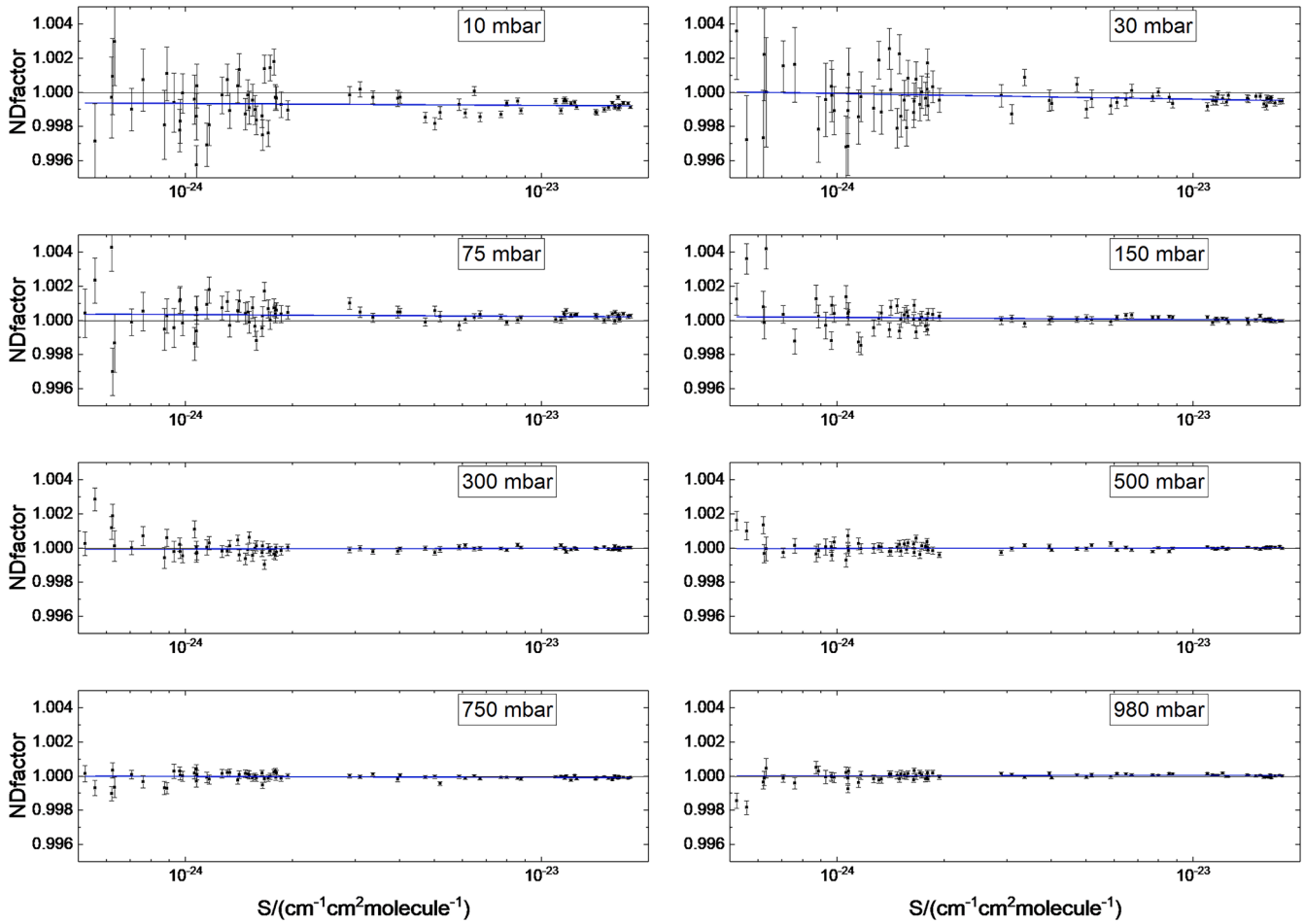

Fig. 2. Number density factors (*NDfactor*) vs. line intensity. 1σ statistical uncertainties shown. A straight line fitted to the datapoints is shown in blue.

Table 4
Averaged number density factors (*NDfactor*) together with χ of averaging. The measurement number corresponds to Table 1. Errors in parentheses are a priori uncertainties calculated from *NDfactor* uncertainties.

Meas.	*p*/mbar	Average *NDfactor*	χ
1	10	0.999230(23)	1.66
2	30	0.999587(37)	1.10
3	75	1.000239(24)	1.18
4	150	1.000056(18)	1.29
5	300	0.999985(13)	1.19
6	500	1.000005(11)	1.19
7	750	0.9999299(93)	1.22
8	980	1.0000303(87)	1.30

exponent and the depletion may be too small by 0.03 and 2.3 %, respectively. This estimation is a worst case since it uses the maximum inhomogeneity, and furthermore, the assumption of a fraction of gas at ambient temperature is the inhomogeneity scenario with largest error impact. For the other parameters no assessment of inhomogeneity error propagation was made. The systematic and statistical uncertainties for the depletion at 212 K is given in the database. Since the uncertainty for the temperature exponent is constant for all lines it is not given in the database.

The 10 mbar, 212 K measurement is useful to assess the validity of the measurements and analysis. At 10 mbar the depletion is negligible and the number density/temperature fit should deliver a number density factor of 1. In the fit of this spectrum, the ambient temperature/low temperature database was used as input and only line intensities and $n_{\gamma 2,self}$ were fitted. Since the ambient temperature ILS was used, $n_{\gamma 2,self}$ is an effective ILS patch to remove most of the residuals. The fitted number density factor is 0.999801(39), which shows that the low temperature measurement is in excellent consistency with the ambient temperature line intensities, including the temperature conversion of line intensities. The fitted temperature was even 0.2 K lower than the cell temperature (see Table 2), caused by the mirror temperatures being 2.2 K lower than the cell body. At this pressure of 10 mbar, there is no impact of the ambient temperature flanges on the gas temperature in the beam path (see above).

As done for the ambient temperature analysis, number density factor fits were carried out to assess the quality of the database. The results are shown in Fig. 3. The *NDfactors* depend on the considered line intensity and differ from 1 by up to 0.2 % for weak lines. This again shows that the quality of the fit is not as good as that for ambient temperature (see Fig. 3), likely due to the temperature inhomogeneity.

3.1.7. CO_2 self-continuum retrieval

As stated above, only the ambient temperature measurements were carried out first and the 212 K experiments were made later. The following investigations to improve and assess the continuum were thus carried out with the ambient temperature data only.

As in [7] the continuum is determined from the baselines in each microwindow fit. The baselines are transmittance polynomials multiplied with the calculated line transmittance to fit the observed spectrum. In the present case the microwindows used in the line parameters fit are too broad to represent the continuum with sufficient resolution. Therefore, two sets of microwindows with smaller spectral ranges were used, the first with a width range of 1–3 cm^{-1} and the second with a width range of 3–4 cm^{-1}. The smoothest continuum was obtained with

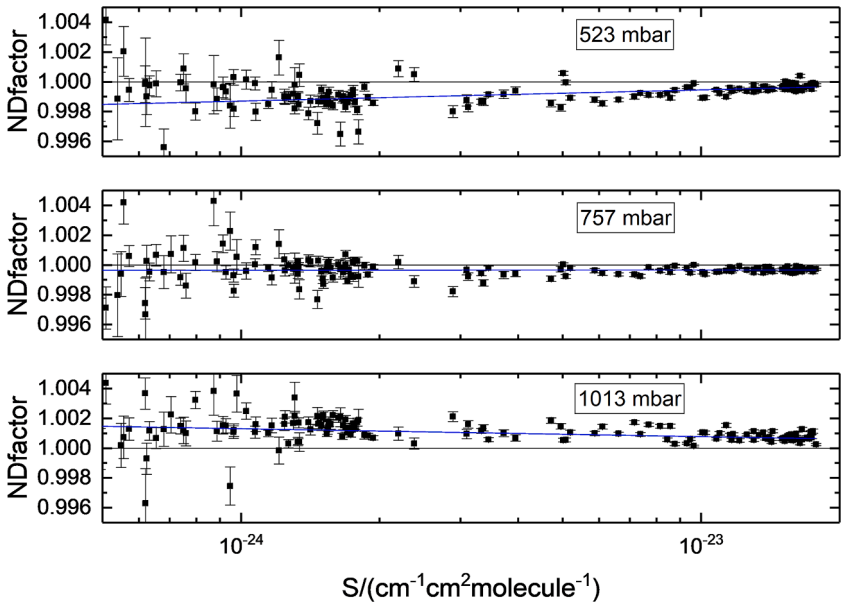

Fig. 3. Number density factors (*NDfactor*) vs. line intensity for 212 K measurements. 1σ statistical uncertainties shown. A straight line fitted to the datapoints is shown in blue.

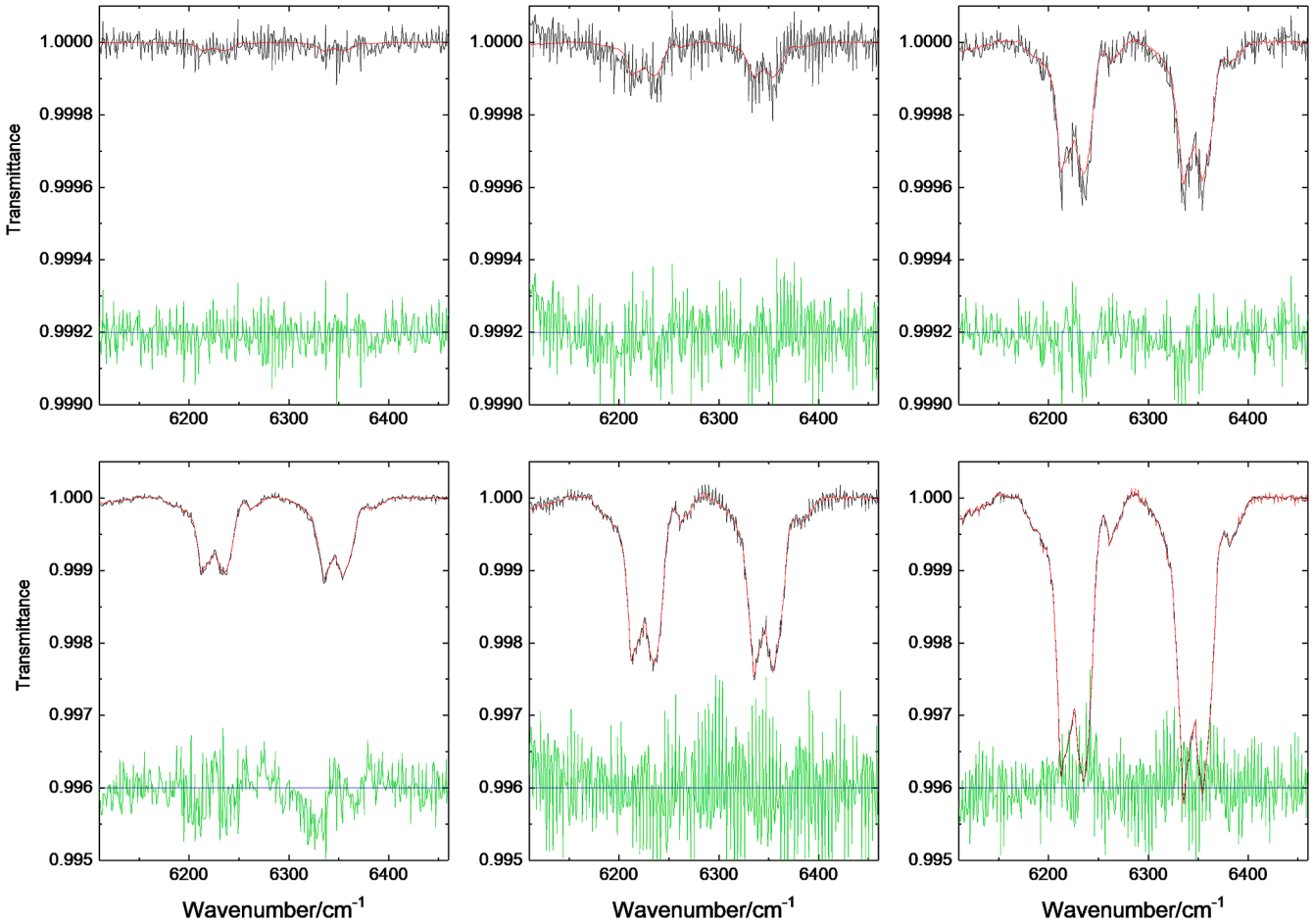

Fig. 4. Self-continuum fit from pure CO_2 measurements (from top left to bottom right measurements #3 (75 mbar), #4 (152 mbar), #5 (299 mbar), #6 (505 mbar), #7 (753 mbar), and #8 (987 mbar) in Table 1). Black: corrected observed baselines, red: calculated baselines, green: (observed-calculated) × 2 (top row), (observed−calculated) × 10 (bottom row), blue: zero line for green trace. Note the different transmittance scales among the plots.

the 3–4 cm^{-1} width microwindows. In these fits the line parameters were kept unchanged (set to the values obtained as explained above) and the wavenumber calibration, number density, and a quadratic baseline polynomial were adjusted. The number densities serve as quality check and were discussed in the Sections 3.1.5 and 3.1.6, "Line parameter uncertainties from ambient/low temperature measurements". First, it was investigated whether this procedure is justified by inspecting the residuals. In order to check whether there is still continuum information present in the residuals for each spectrum separately, the concatenated residuals of all microwindows were convolved with a Gauss function of 5 cm^{-1} FWHM to improve the signal-to-noise ratio. It was found that the smoothed residuals show features which are smaller than 0.1 % of the continuum absorption. The unconvolved residuals as well as convolved residuals with a 1 cm^{-1} FWHM Gauss function do not show higher resolution continuum information.

Baseline spectra, containing the continuum information, were calculated concatenating the baseline polynomials for each microwindow for each spectrum in the range 5980–6570 cm^{-1}, choosing a sufficiently fine spectral sampling of 0.1 cm^{-1}. The results show imperfections due to drifts in the instrument between sample and reference measurements. These imperfections are very low-resolution deviations from the 100 % level. To correct this, continuum-free ranges (6150–6170, 6282.5–6290.5, 6412–6450 cm^{-1}) were selected (see blue bars in Fig. 9) and a 3rd order polynomial in wavenumber was fitted for all three ranges together for each spectrum individually in order to represent the entire continuum-free baseline transmittance spectrum. For each spectrum, the original concatenated baselines were then corrected by dividing them by the corresponding polynomial. After this, the continuum coefficients were fitted for each spectral point in the range 6110–6460 cm^{-1} to the corrected baseline transmittance spectra according to [7]. The statistical uncertainties of the 0th order baseline coefficients (resulting from the multispectrum fit) were applied for weighting. The observed, calculated, and residual spectra are shown in Fig. 4. The measurements #1 and #2 with negligible continuum information were considered in the fit but are not shown in the figure. The residuals still show some systematic features, likely caused by imperfections of the baseline correction. An excerpt of the resulting continuum is shown in Fig. 5. The statistical uncertainty from the fit is also shown in the figure. It shows strong variations within individual microwindows, with the largest values always near the microwindow edges because there the polynomial representation of the baseline has its largest uncertainties. Indeed, in Fig. 5 discontinuities located at the borders of microwindows are visible. Thus, the arbitrary selection of microwindows leads to an also arbitrary strong wavenumber-dependent variation of the continuum uncertainty.

In order to solve this problem, the spectrum was cut into two sets of microwindows, both consisting of 3 cm^{-1} wide microwindows, but one of them shifted by 1.5 cm^{-1}. The resulting continua were averaged, taking the respective uncertainties into account, leading to the results in Fig. 9. The statistical uncertainty of the fit, which is based on the residuals, contains systematic errors in the baseline correction.

A further test was carried out to confirm the validity of the microwindow width selection. The procedure described for the 3 cm^{-1} wide microwindows was repeated for a width of 1.5 cm^{-1} and a shift of 0.75 cm^{-1}. A noisier continuum resulted, not showing higher resolution signatures. Thus, the 3 cm^{-1} microwindow width selection was maintained.

Figs. 6 and 7 give an impression of the continuum together with the line absorption for the highest pressure. The baseline correction polynomial is at about 99.8 % transmittance, the continuum has about 0.4 % absorption. The line absorption is up to 90 % and in the region of the continuum significantly larger than the continuum, even in the valleys between lines. The small impact of the continuum on the total spectrum can be seen in Fig. 7. This shows that the continuum is buried under the line spectrum and that continuum and line parameters have to be determined from the same spectra [7].

The observed, calculated, and residual spectra at 212 K are shown in Fig. 8. The continuum absorption is about five times larger than the value at ambient temperature (Fig. 4). Systematic residuals are present, changing sign from 500 to 1000 mbar, of about 10 % and 2 % at 500 mbar and 1000 mbar, respectively. This could partly be caused by the temperature inhomogeneity. Since the continuum fits arise from baselines obtained from line parameter fits showing residuals due to inhomogeneity, this may induce another (indirect) error source linked to the inhomogeneities. The impact of the residuals is included in the uncertainties in Fig. 9.

In Fig. 9 the continua at 294 and 212 K are shown. Obviously, the 212 K continuum is significantly larger. The small structures to the right of the main bands are larger at low temperature but decrease relative to the continuum maximum. A small structure appears to the left of the 30013 band. In contrast to the 294 K continuum, the uncertainties at 212 K are increased in the regions with large continuum intensity. This is linked to the residuals in Fig. 8. It is remarkable that the continuum shapes for the 30012 and 30013 bands are very similar. This supports the validity of the baseline correction.

4. Intensity correction, continuum, and second virial coefficient

Linear decrease of experimentally retrieved line intensity with increasing pressure for CO_2 has been detected for the first time. In order

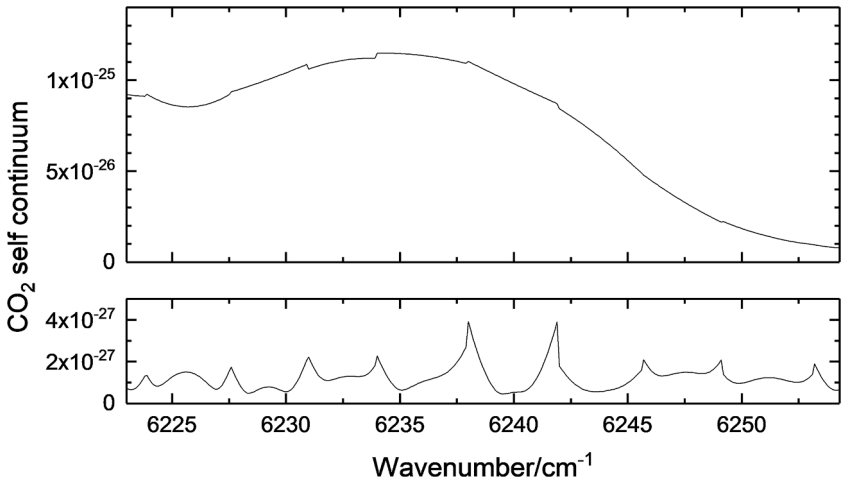

Fig. 5. Excerpt of continuum in $cm^2 molecule^{-1} atm^{-1}$. Upper graph: Continuum fitted with microwindows 3–4 cm^{-1} wide, lower graph: Statistical uncertainty from fit times χ. The strong variation of the uncertainty is most visible in the microwindow 6238–6242 cm^{-1}.

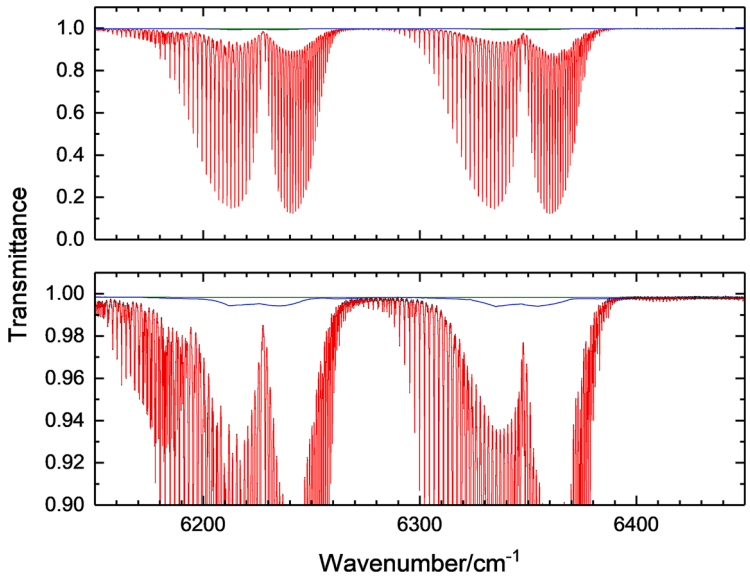

Fig. 6. Contributions to calculated transmittance.Black: measured (#8 in Table 1, 987 mbar), red: calculated, green: baseline correction polynomial, blue: continuum × baseline correction polynomial.

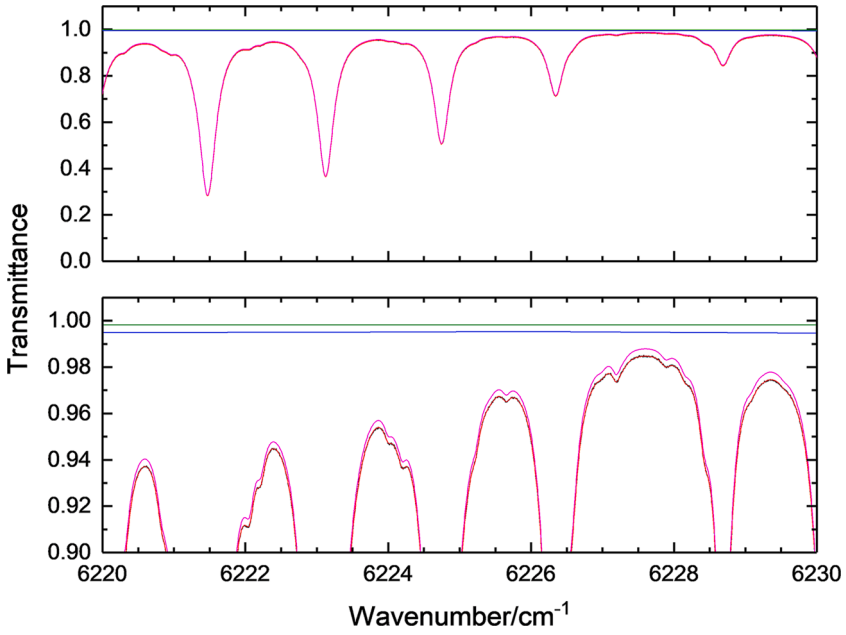

Fig. 7. Zoomed region from Fig. 6. Additionally shown in magenta: calculated without continuum.

to check for the linearity with pressure of the retrieved intensity at each pressure, i.e. $S(p)$, we multiplied the fitted number density factors for each spectrum and microwindow (see Fig. 2) with $(1+d_{self}\times F_{p\text{-}corr}\times p_{CO2}[\text{mbar}]/1013.25)$, where d_{self} is the average fitted correction in each microwindow. This product corresponds to $S(p)/S(p=0)$. Fig. 10 shows two examples for the linearity of the PDIC vs. pressure for ambient temperature. The linearity is excellent, justifying the definition of d_{self} and its usage in the multispectrum fitting. The values of d_{self} at ambient temperature for the four bands 30011, 30012, 30013, and 30014, together with their statistical uncertainties are displayed in Fig. 11. All four bands show a very similar m-dependence ($m=-J''$ in P-branches, $m=J''+1$ in R-branches). As in case of CO [28] and HCl [37,38], a large $|d_{self}|$ value occurs for low m quantum numbers and it decreases with $|m|$. In contrast to CO and HCl, here $|d_{self}|$ increases again in the R-branch for CO_2. In the P-branch for high values of $|m|$, $|d_{self}|$ slightly increases. Fig. 12 shows d_{self} for 212 K. They are significantly larger when compared to ambient temperature and show a partly different m-dependence. While they are still large for low m, there is only a slight increase in the R-branch with higher m and a steady decrease in the P-branch. At 212 K d_{self} has about the same magnitude as the largest one so far reported in the literature, observed for pure HCl [37] and HCl in CO_2 [37].

An important question was whether the missing intensity can be found in the continuum, i.e. whether the continuum is part of the line profile not covered in the line model. This can be investigated by comparing the intensity-weighted intensity correction parameters $d_{self,av,fit}$ and the area of the continuum divided by the band intensity, $F_{cont\text{-}area}$. However, the results, as obtained by the multispectrum and continuum fits, cannot be directly compared since in the line fit the profiles are normalized as if extending to infinity, but for the continuum

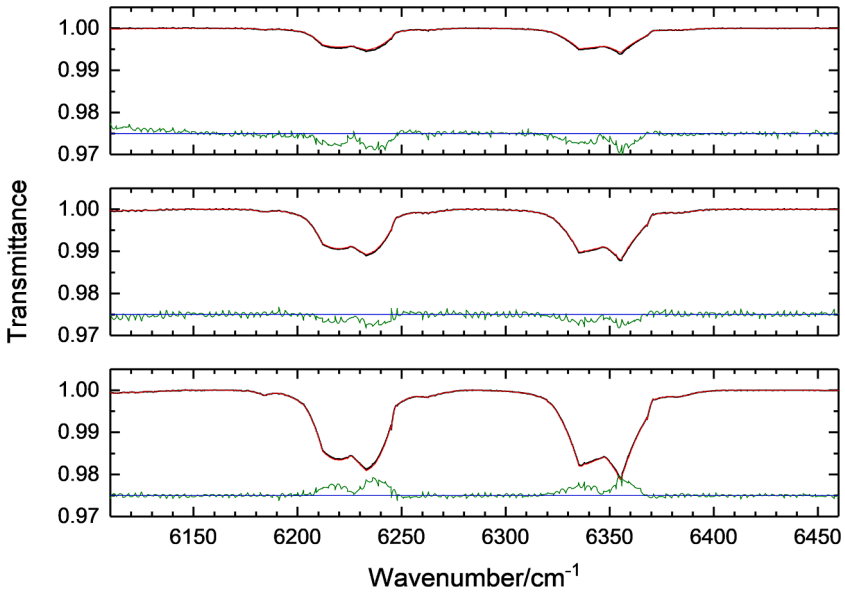

Fig. 8. Self-continuum fit from 212 K pure CO_2 measurements (from top to bottom measurements #12 (523 mbar), #13 (757 mbar), and #14 (1013 mbar) in Table 2). Black: corrected observed baselines, red: calculated baselines, green: (observed-calculated) × 10, blue: zero line for green trace.

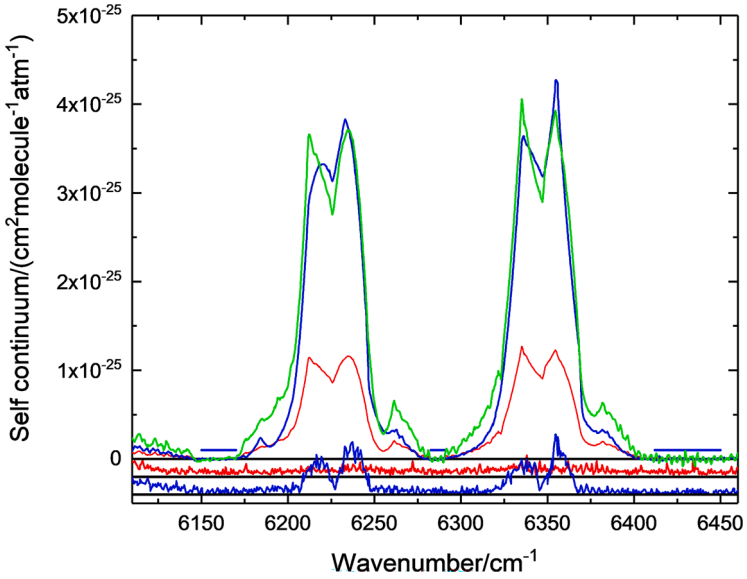

Fig. 9. CO_2 self-continuum of the 30012 and 30013 bands, red 294 K, green 294 K x 3.2, blue 212 K. The statistical uncertainty is multiplied by 10 and offset by -2×10^{-26} for 294 K and -4×10^{-26} for 212 K. Regions for baseline correction are marked in blue. Zero lines for the respective traces are shown in black.

determination, they are cut at ±25 cm^{-1} from the line center. The truncation present in the multispectrum fitting does not affect the line parameters and hence the depletion, since the core of the line is not affected by the truncation and the truncation only affects the fitted baseline and thus the continuum. In order to make depleted intensity and continuum comparable, either the continuum or the intensity correction parameters have to be corrected. We tried to correct the continuum by subtraction of line profiles beyond ±25 cm^{-1} but this resulted in ranges with negative continuum and the baseline correction would not work. Alternatively, the normalization of the line profiles needs to be corrected. For a single line a correction factor F_{Scorr} of the line intensity can be calculated from the infinity-normalized line profiles $f(\sigma,p)$ with wavenumber σ and pressure p:

$$F_{Scorr} = \frac{1}{\int_{-25\ cm^{-1}}^{+25\ cm^{-1}} f(\sigma,p)d\sigma}$$

The corrected average intensity correction parameter $d_{self,av,corr}$ is given by

$$d_{self,av,corr}\cdot p = d_{self,av,fit}\cdot p - \left(1 - \sum_{band}\left(S\cdot \int_{-25\ cm^{-1}}^{+25\ cm^{-1}} f(\sigma, 1\text{atm})d\sigma\right) \Big/ \sum_{band} S\right)\cdot \frac{p}{1\text{atm}}$$

The correction term is approximately proportional to the pressure for pressures below 1 atm. The equation can be simplified by dividing by the pressure but p is left in for clarity. The correction is about 0.0025 atm^{-1} at 294 K and 0.0032 atm^{-1} at 212 K for the 30012 and 30013 bands. The comparison with the real gas number density correction (see below) requires population-weighted average depletions. It was found that intensity and population weighting give nearly the same results, thus only intensity-weighted results are given here.

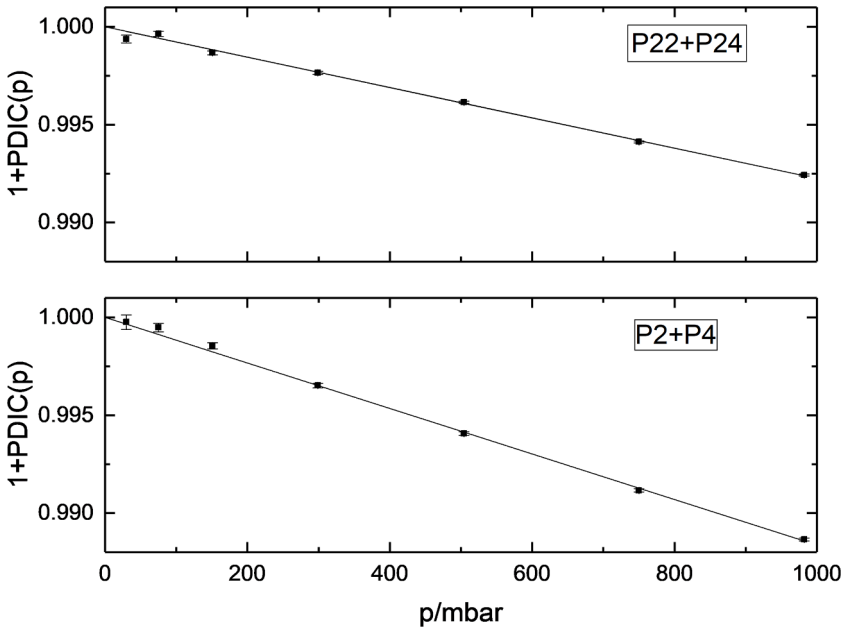

Fig. 10. Pressure-dependent intensity correction factors (1+PDIC) as function of pressure for individual measurements for two microwindows in the 30012 band at room temperature with 1σ statistical uncertainties. 1+PDIC as calculated from the d_{self} parameters is also shown (straight line). The microwindow spectral ranges are 6325.9–6329.8 cm^{-1} (P22+P24) and 6344.0–6347.8 cm^{-1} (P2+P4).

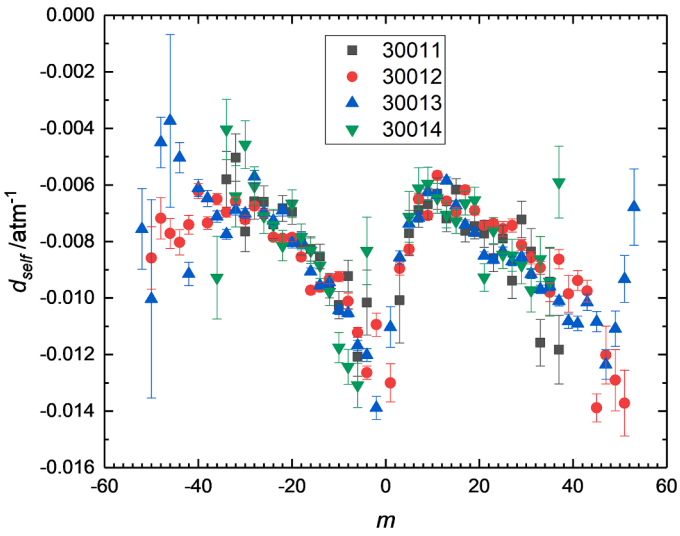

Fig. 11. Ambient temperature d_{self} for the four 3001x (x = 1,2,3,4) bands vs. m with 1σ statistical uncertainties.

There is a physical justification to use cut line profiles in the multi-spectrum fitting. It is well known that the impact approximation fails in the far line wings leading to sub-Lorentzians [13] due to finite duration of collisions (non-impact effects).

The line intensities are summed in the spectral regions covered by the bands, thus including lines of hot bands, isotopologues, etc. Thus, in the continuum, weak other bands are included, while for calculation of the average intensity correction parameter, only the main bands are considered. This is justified since the hot bands etc. are weak and the vibrational/isotopologic dependence of intensity depletion and continuum is expected to be small.

The results are given in Table 5. The normalization correction is about 24 % for 294 K and 11 % for 212 K. The difference arises from the ca. three times larger average depletion at 212 K, while the absolute correction has only a small temperature dependence (see above). There is a very good agreement (0–10 % difference) between $d_{self,av,corr}$ and continuum areas for both bands and both temperatures.

In Table 5 the number density correction $F_{n\text{-}corr}$ for 1 bar calculated from the Soave-Redlich-Kwong formulation (see Section "Experiment") is given. In case this number density correction is linked to dimerization decreasing the number of monomers, the average intensity correction parameter is predicted by $d_{self,av,pred} = 2/F_{n\text{-}corr} - 2$, the value of $d_{self,av,pred}$ is reported in Table 5 as well. There is a good agreement (0–7 % difference) for $d_{self,av,corr}$ and continuum areas with the intensity correction calculated from the real gas number density correction. Note that the good agreement was observed when using a line profile truncated at ±25 cm^{-1}. In case no truncation is applied the $d_{self,av}$ values in the first row of Table 5 would have to be used, which are smaller than the predictions from the number density correction, specifically by 20 % at 294 K and 7 % at 212 K. The good agreement for the truncated profile may indicate that the 25 cm^{-1} cut is closer to the truth (breakdown of impact approximation, see above) than the uncut line profile.

It is well known that the real gas number density correction can also be calculated from the 2nd virial coefficient. For example, applying 2nd virial coefficients from [16] the number density correction agrees within the percent level with the SRK correction. Since in combination with continua and dimerization, especially for H_2O, the 2nd virial coefficient is involved [32] and there is also a theoretical access via the intermolecular potential [10], which is also linked to the dimerization [39], we also consider it in combination with PDIC and continuum.

It was investigated how the continuum fit would have been affected if the line profiles had been calculated to infinity. The middle spectral interval used for baseline correction in the continuum fit (see Fig. 9) would show significant absorption which would affect the shape of the baseline polynomials. The effect would increase with pressure. The baseline polynomials did not show such an effect. Thus, we can conclude that there is no noticeable line wing contribution beyond 25 cm^{-1}. Since 25 cm^{-1} is arbitrary, we tested what would have happened if multi-spectrum fitting had been carried out with a 20 cm^{-1} cut-off. This effect could not be observed in the baseline and the normalization correction would be larger by 0.0006 atm^{-1} for ambient temperature, which is about 25 % of the correction applied (see above). The findings in this paragraph support that the selection of the 25 cm^{-1} cut-off is indeed

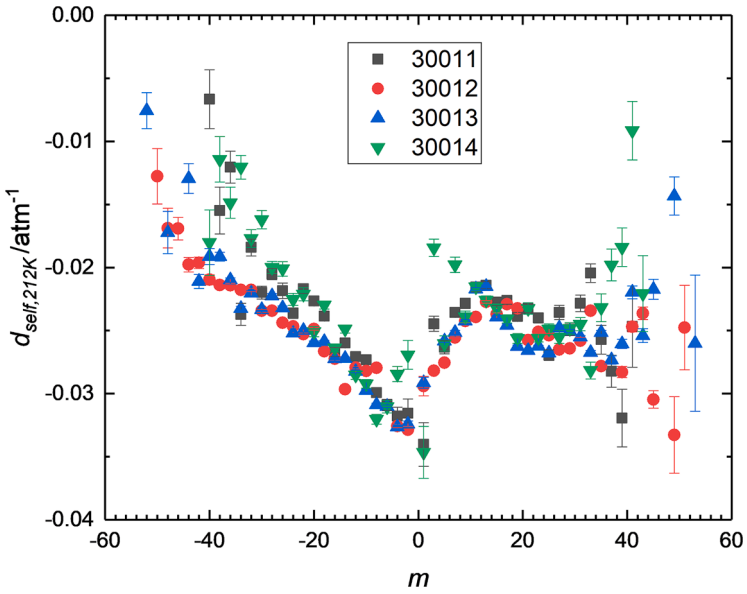

Fig. 12. $d_{self,212\ K}$ for the four 3001x (x = 1,2,3,4) bands vs. m with 1σ statistical uncertainties.

Table 5
Uncorrected and corrected averaged intensity-weighted intensity correction parameters ($d_{self,av,fit}$ and $d_{self,av,corr}$), integrated continua fraction ($F_{cont\text{-}area}$), real gas number density correction for 1 atm ($F_{n\text{-}corr}$), and average intensity correction parameters predicted from real gas number density correction ($d_{self,av,pred}$). Summation/integration ranges are 6285–6410 cm^{-1} and 6155–6285 cm^{-1} for the 30012 and 30013 bands, respectively. Note, that depletions are negative and continuum areas positive.

		294 K		212 K	
	truncation	30012	30013	30012	30013
$d_{self,av,fit}$/atm^{-1}	none	−0.008047(30)	−0.008220(29)	−0.02564(13)	−0.026437(79)
$d_{self,av,corr}$/atm^{-1}	@25cm^{-1}	−0.01053	−0.01069	−0.02886	−0.02965
$F_{cont\text{-}area}$/atm^{-1}	@25cm^{-1}	0.01018	0.00978	0.02894	0.02747
$F_{n\text{-}corr}$		1.00525	1.00525	1.01423	1.01423
$d_{self,av,pred}$/atm^{-1}		−0.01045	−0.01045	−0.02806	−0.02806

realistic, supporting the validity of the comparison of intensity correction parameters and continuum areas with estimations from real gas number density corrections.

From the agreement of $d_{self,av,corr}$ and continuum areas it follows that the integral band intensity including the continuum stays constant with pressure. The continuum can be seen as dump for incomplete line modelling. Note that the continuum shape is pressure-independent. Otherwise, the plots in Fig. 4 would show systematic residuals, continuously changing with pressure. Thus, the continuum contains line profile contributions with pressure independent shape. Presently, an extended line model including such contributions is not available. Such an extended line shape model would not require any intensity correction. It should be emphasized that in the present multispectrum fitting the most sophisticated line shape model was used. The only simplification is the use of the Rosenkranz line mixing approximation. In order to check this simplification, synthetic spectra were computed using the full relaxation matrix for the line mixing [14,35] and fitted using the Rosenkranz approximation. Neither PDIC nor a continuum was found, clearly showing that the relaxation matrix does not model these effects. The missing line shape contribution is of very low resolution, appearing in the fitted baselines when cutting the spectra into microwindows. Therefore, state-of-the-art spectrum processing produces line parameters with intensity depletion and a continuum. Depleted intensity quantitatively transferred to a continuum has been observed for the first time.

It was attempted to fit the continuum as a sum of broad, pressure-independent Lorentzian line shape contributions. The model contains Lorentzians multiplied with the depleted intensities with normalization corrections for individual lines. For the Lorentzian halfwidth a linear dependence on the m quantum number was defined applying two parameters, the Lorentzian halfwidth Γ_{super} at $m = 0$ and a slope (change of the Lorentzian halfwidth with $|m|$): $\Gamma_{super}(m) = \Gamma_{super}(m = 0) + |m| \cdot \Gamma_{super\text{-}slope}$. Since the continuum P- and R-branch shapes were narrower than the band shape, first order pressure-independent line mixing, applying the Lorentzian halfwidth $\Gamma_{super}(m)$, was added, having a linear m dependence with a value of 0 atm^{-1} at $m = 0$: $Y_{super}(m) = m \cdot Y_{super\text{-}slope}$. Additionally, a scaling factor was fitted for the Lorentzian contribution, $SC_{\Gamma\text{-}super}$. The parameters were common for both bands, 30012 and 30012. Observed and modelled continuum for both temperatures are displayed in Fig. 13 and fitted parameters are in Table 6. The scaling factors for the Lorentz contribution are very close to 1, showing that the depleted intensity indeed goes into the continuum (in line with the intensity-weighted average depletion and the continuum area, see Table 5). The line mixing does not contribute to the area. The super-Lorentzian halfwidth increases from 1.17 cm^{-1} (1.91 cm^{-1}) for m = 0 to 13.7 cm^{-1} (10.9 cm^{-1}) for $|m|$=50 for 294 K (212 K). Note that a large increase of Γ_{super} with m was also observed from rCMDS calculations for HCl (Fig. 11c in [37]). The agreement of observed and modelled continuum is not too good, but the goal was to show that super-Lorentzian line profiles with pressure-independent shape (constant Lorentzian width) can reproduce the continuum, applying the depleted intensity from standard line modelling. Anyhow, given the crudeness of the model, the agreement is reasonable.

It is remarkable that for the foreign continuum of water in the 3 μm region [7] P- and R-branch shapes were narrower than the band shape, too. The small features to the right of the bands are not covered in the

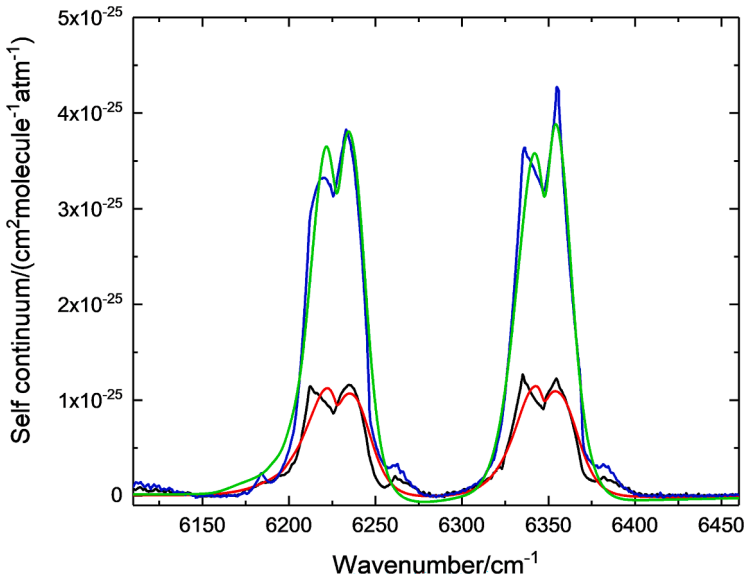

Fig. 13. Observed (294 K black, 212 K blue) and modelled (294 K red, 212 K green) CO_2 self-continuum.

Table 6
Fitted parameters to model continuum with super-Lorentzian contributions. $SC_{\Gamma\text{-}super}$: scaling factor for super-Lorentzians, $\Gamma_{super}(m = 0)$: super-Lorentzian half width for $m = 0$, $\Gamma_{super\text{-}slope}$: slope of super-Lorentzian half width with $|m|$, $Y_{super\text{-}slope}$: slope of super-Lorentzian first order line mixing with m. Note: Y_{super}=0 for $m = 0$.

Parameter	294 K	212 K
$SC_{\Gamma\text{-}super}$	0.970	0.960
$\Gamma_{super}(m = 0)$	1.17 cm^{-1}	1.91 cm^{-1}
$\Gamma_{super\text{-}slope}$	0.25 cm^{-1}	0.18 cm^{-1}
$Y_{super\text{-}slope}$	−0.00270	−0.00305

model and might be bound dimer bands which are expected to have a narrower band shape due to the smaller rotational constants.

5. Retrieval simulations

Simplified retrieval simulations of satellite observations are helpful to determine the required accuracy of the spectroscopic database in order to achieve the targeted accuracy of the atmospheric data product, e.g. CO_2 column (XCO2). Such simplified retrieval simulations were introduced by DLR in the SEOM-IAS project [31] for Sentinel-5P observations of CH_4 and CO and were then applied to the CO2M mission in the ISOGG project [21]. The CO2M retrieval simulations were extended to investigate the impact of the PDIC and the continuum. Temperature-dependent CO_2/air intensity correction parameters d_{air} and continua were obtained by scaling the ambient temperature CO_2 results from the present work. In case of d_{air} m-dependent averages from the four bands 30011, 30012, 30013, 30014 were calculated, while in case of the continuum 30012 and 30013 results were averaged. The scaling factors for the continua were obtained from temperature-dependent 2nd virial coefficients calculated by integration of the Lennard-Jones potential (see discussion). At ambient temperature the air-broadened continuum is about three times smaller than the self-continuum. The temperature dependence is parameterized by applying a factor $(296\ K/T)^{3.4}$. The continuum is placed according to the band centers of the three 2 μm and the four 1.6 μm bands and further scaled according to the respective band intensities. For intensity correction parameter normalization corrections for pure CO_2 and air were considered, applying the experimentally determined broadening parameters. The temperature dependence could be parameterized as 3rd order polynomial. The d_{air} are smaller than the d_{self} values by a factor of 0.45, mostly independent of temperature and m quantum number.

The retrieval simulations are described as follows. Radiative transfer is strongly simplified. Clear sky transmittance spectra without scattering through a layered atmosphere, typically 8 layers, for NADIR observation are calculated, including an airmass factor, typically 3. The atmospheric state is represented by standard AFGL profiles [1]. Three cases are considered: tropical atmosphere (TRO) with ground altitude 0 km, subarctic winter atmosphere (SAW) with ground altitude 0 km, and tropical atmosphere with ground altitude 2 km. Monochromatic transmittances are calculated using a partially correlated quadratic speed dependent Voigt profile together with first order Rosenkranz line mixing for CO_2 and interfering H_2O. The MTCKD 3.2 H_2O continuum is applied. The spectra are convolved with the instrumental line shape function for the spectrometer on CO2M assuming a Gauss shape. The retrieval of XCO2 and XH2O involving a least squares fitting procedure is carried out with a perturbed spectroscopic database. A baseline polynomial is also fitted.

There are two different uncertainty types relevant for atmospheric retrieval, a global bias and a differential uncertainty. For the global bias the allowed spectroscopical error contribution is 0.5 %, and 0.03 % for the differential uncertainty. The differential uncertainty specifies the maximum difference in the CO_2 column introduced by spectroscopic database errors for different atmospheric conditions. In the present case the most different atmospheric conditions arise for tropical and subarctic winter climatology as well as ground altitudes of 0 and 2 km. Furthermore, spectroscopic errors should not introduce residuals larger than 0.08 %.

CO2M uses two spectral regions for CO_2 column determination, the 1.6 μm region (strongest band to be used is 30013), in which CO_2 bands are investigated in the present paper, and the much stronger 2.0 μm region. There are two bands of interest for CO2M, the 20012 and 20013 bands, being 17 and 75 times stronger than the 30013 band, respectively. Retrieval simulations were carried out for both spectral regions in order to investigate the impact of depletion and continuum for the differently strong bands relevant for CO2M satellite observations.

In order to quantify the impact of the intensity depletion and the continuum, “measured” atmospheric spectra were calculated with continuum, with depletion and with both, continuum and depletion. In the retrieval, continuum and depletion were switched off. The results on bias and residuals for tropical atmosphere are summarized in Table 7 and the results on differential error in Table 8 and an example for the

Table 7
Impact of depletion and continuum on CO_2 column and peak-to-peak (p-p) residuals in simulated CO2M retrievals for tropical atmosphere for 1.6 μm and 2.0 μm regions.

Impact of	1.6 μm (5970–6289 cm^{-1})		2 μm (4773–5025 cm^{-1})	
	CO_2 col. fact.	p-p residual/ %	CO_2 col. fact.	p-p residual/ %
depletion	0.9983	0.02	0.9983	0.03
depletion+cont	1.0029	0.10	1.0148	1.1
cont	1.0046	0.10	1.0165	1.1

Table 8
Differential CO_2 column error between tropical and subarctic winter atmospheres and for tropical atmosphere between 0 km and 2 km ground altitude for 1.6 μm and 2.0 μm regions.

Impact of	1.6 μm		2.0 μm	
	TRO−SAW/ %	TRO(0 km−2 km)/ %	TRO−SAW/ %	TRO(0 km−2 km)/%
depletion	0.1262	0.0041	0.1484	0.0051
depletion+cont	−0.0559	0.0320	−0.4735	−0.0383
cont	−0.1825	0.0328	−0.6230	−0.0425

"measured" satellite spectrum and the residuals in the 1.6 μm region is shown in Fig. 14. The depletion alone gives a CO_2 column bias of −0.2 % for the 1.6 μm and 2.0 μm regions, the continuum alone of +0.5 % and +1.7 %, and the total impact of depletion and continuum is +0.3 % and +1.5 %, respectively. The impact of depletion and continuum is within the total error budget for the 1.6 μm region, but significantly outside for the 2.0 μm region. The impact of depletion and continuum is as expected opposite in sign and the impact of continuum is larger than that of depletion. Thus, considering only the depletion in the spectroscopic data base would lead to a worse result than leaving out depletion and continuum. Certainly, the best results require continuum and depletion in the atmospheric retrieval. The residuals are considerably larger in the 2.0 μm region when omitting the continuum. Residuals exceed the requirements by about a factor 13 in the 2.0 μm region. The differential error for TRO−SAW exceeds the requirement in the 1.6 μm region by a factor 2 and in the 2 μm region by a factor 16. In case of the TRO(0 km−2 km) differential error requirements are met in the 1.6 μm region and slightly exceeded in the 2 μm region. The reason for the different impact of the continuum in the 1.6 and 2.0 μm regions is the larger optical depth in the 2.0 μm region with already strongly opaque CO_2 signatures. The optically thin continuum absorption gains more weight with respect to the opaque line spectrum. In case of the OCO mission the strongest band 20012 in the 2.0 μm region is omitted, decreasing opacity, and the spectral range is reduced to 4773–4880 cm^{-1}. The maximum bias drops from +2 % (SAW) to −0.27 %, while the differential error (TRO−SAW) drops from −0.5 % to +0.13 % when compared to the CO2M spectral range. The impact is smaller but still significant. In conclusion, the continuum is very important for satellite spectra retrieval. In order to avoid large systematic errors, the continuum must be implemented in the processing of atmospheric spectra, together with the depletion.

6. Discussion

6.1. Intensity correction and continuum

The most interesting result of the present work is the agreement of the normalization-corrected, intensity-weighted average intensity correction parameter ($d_{self,av,corr}$), the continuum area ($F_{cont\text{-}area}$), and the $d_{self,av,pred}$ calculated from the real gas number density correction. The agreement for two different temperatures makes a coincidence unlikely. Initially, the agreement of $d_{self,av,pred}$ is surprising, since Serov et al. [32] excluded that super-Lorentzian line wings, contributing to the water in-band self-continuum, are linked to part of the second virial coefficient (see Introduction). Moreover, Serov at al. introduced super-Lorentzian line wings to account for a continuum too large to originate from bound and quasi-bound dimer only, both of which contribute to the second virial coefficient. However, super-Lorentzian line wings are proven by rCMDS calculations (see Introduction) to be, at least partly, the origin of the PDIC. The rCMDS calculations use an intermolecular potential which also yields a second virial coefficient. In case of CO_2, Bock et al. [10] have calculated an intermolecular potential and derived a 2nd virial coefficient. This coefficient yields a number density correction in very good agreement with that in Table 5. Both, a negative

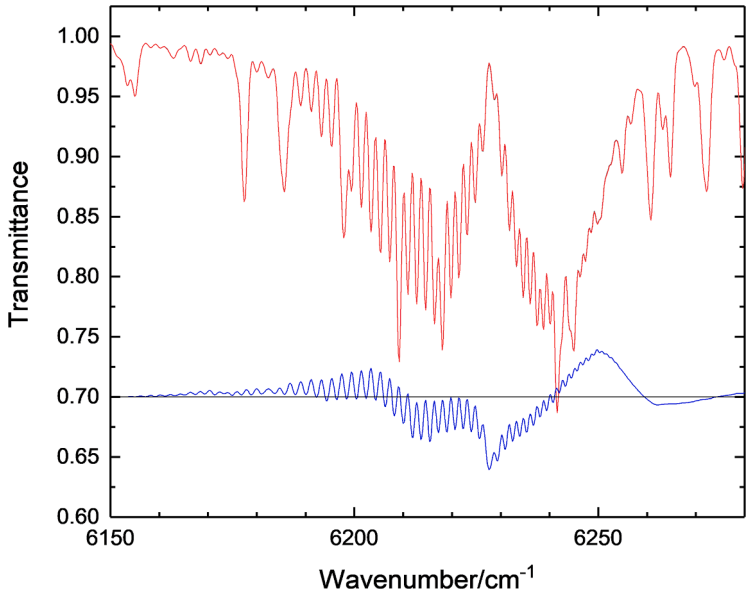

Fig. 14. Excerpt of "measured" with continuum and depletion (black, covered by fitted) and fitted without continuum and depletion (red) CO2M satellite spectrum in the 1.6 μm region for tropical atmosphere, airmass factor 3. Residuals multiplied by 100 and offset by 0.7 are shown in blue. The corresponding fitted CO_2 columns together with the peak-to-peak residual are in the second line of Table 7. The shape of the residuals arises mostly from the shape of the continuum, which is different from band shape and the fit tries to compensate by adjusting the line spectrum intensity.

second virial coefficient and non-Markovian collisions, are linked to a minimum in the intermolecular potential. This supports that super-Lorentzian line wings are linked to the second virial coefficient. How can the results presented here be combined with the results on CIA (see Introduction)? From Fig. 6 in [40], the intensity contribution of bound CO_2 dimer is ca. 20 % and 11 % for 210 K and 296 K, respectively. A clear CO_2 bound dimer structure as in [40] and [3] is not observed in the present data, but also not in [4]. Moreover, the $\nu_2+\nu_3$ CIA could be modelled from monomer transitions with modified selection rules. The 1.6 μm bands have the involvement of the asymmetric stretch ν_3 in common, whereas there is no ν_3 involved in the Fermi dyad and triad. Either the intensity of the dimer in the Fermi dyad and triad is much stronger than the quasi-bound/free pair CIA, or the contribution of the narrow parallel band type to the dimer spectrum is smaller (broad perpendicular band type dominates). In the latter case the bound dimer band may be buried in the continuum. While non-Markovian collisions could be related to quasi-bound dimers and free pairs, in the total PDIC a fraction may be connected to bound dimer formation not covered by rCMDS calculations. The intensity of bound dimer would in this case be similar to twice that of the monomer.

The intensity-weighted d_{self} are dominated by the m-dependence of the line intensities as is the continuum shape. Since the line intensities are strongly linked to the lower state population, the contributions to the number of "collisional dimers" are also nearly proportional to the line intensities. The term "collisional dimers" was introduced here to indicate that during the collision the molecules stay longer in proximity than expected for the impact approximation due to the minimum in the intermolecular potential.

How do the d_{self} and their m-dependence compare to previous results for HCl [37,38] and CO [28]? Table 9 summarizes the intensity-weighted average intensity correction parameters $d_{self/foreign,av,corr}$ for all relevant recent publications. The normalization correction was carried out as described in Section "Intensity correction, continuum, and second virial coefficient", since in all analyses the line profile was normalized to 1 for an HTP extending to infinity. For the normalization correction the line profile was cut at ±25 cm^{-1}, in case of CO/N_2 at ±40 cm^{-1}. The 2nd virial coefficient used to calculate $d_{self/foreign,av,pred}$ was obtained by integration of the Lennard-Jones potential. The use of the intermolecular potential for the calculation of the 2nd virial coefficient is for example described in [10]. The Lennard-Jones potential was used since it is simple and was found, at least for CO_2, to be sufficiently accurate. Parameters for Lennard-Jones potentials of CO_2, CO, N_2, O_2, including mixing rules for interaction between different molecules were taken from [15] and of HCl from [17]. In case of CO_2 the accuracy of this method was validated by comparing calculated gas number density corrections of CO_2/N_2 mixtures with experiments [12] (<1 % difference of number density correction). For CO_2 the agreement of $B_{2,LJ}$ and values from SRK is better than 4 % with the largest difference at 212 K. In case of HCl a difference of 20 % at 293 K was observed when compared to experimental values [30]. Thus, all the entries in Table 9, where HCl is involved, may have larger uncertainties. Except for HCl-HCl and CO-N_2 the agreement between normalization-corrected experimental and predicted intensity correction parameters is excellent. In case of CO-N_2 the average intensity correction parameter is so small that the normalization correction has the same magnitude as the intensity correction parameter, thus the comparison is questionable. In case of HCl-HCl the observed corrected value is about 3 times larger than the prediction. Interestingly, the experimental as well as the rCMDS intensity correction parameters do not drop towards 0 for larger quantum numbers as they do for HCl-air and HCl-CO_2.

For HCl-CO_2, HCl-He, HCl-HCl, and CO-N_2 there is reasonable agreement between experiment and rCMDS calculations. In all cases the largest $d_{self/foreign,av,corr}$s are found for low m quantum number. In case of HCl-CO_2, HCl-air, and CO-N_2 the $d_{self/foreign,av,corr}$s are about zero at higher m quantum numbers. This is interpreted as non-Markovian collisions on a short time scale, being more efficient for slower rotation. From the rCMDS calculations there should not be a major difference between P- and R-branch. Inspecting the results in the present work, d_{self} drops faster in the R-branch from the band center with increasing m. For higher m the values are about constant in the P-branch and increasing again in the R-branch. The m dependence is thus only partly in accordance with the non-Markovian collision approach. Whether line mixing issues are still involved in spite of the test calculations with the full relaxation matrix (see "Intensity correction, continuum, and second virial coefficient") is open.

Since intensity depletion for CO_2 was observed for the first time, there is no literature data to compare with. CO_2-air continua were obtained for the 1.6 μm and 2 μm regions [21] and CO_2-N_2 continua in the 4.3 μm region were obtained from measurements of [42]. The shape was found to be similar to the CO_2 self-continuum, however, due to baseline errors for these very weak continua, the areas were inconsistent and the continua were not used. Therefore, a CO_2-air continuum was obtained by scaling the CO_2 self-continuum by 0.35. The scaling factor was derived from 2nd virial coefficients of CO_2-CO_2, CO_2-N_2, and CO_2-O_2, which were obtained from Lennard-Jones potential integration. The ambient temperature experimental self-, foreign-, and MT_CKD foreign-continua are displayed in Fig. 15. It can be seen that the MT_CKD continuum has about the same magnitude as the CO_2-air continuum, but does not show P- and R-branch and has broader wings.

6.2. Line intensities

The line intensities of the present work are compared with those of our previous work [8]. Fig. 16 shows the intensity ratio of new and old data vs. the line intensity. The systematic uncertainty of the old work is 0.15 %, and of the present work is 0.06 %. The fitted line represents an average difference as function of line intensity. For most transitions the straight line differs from zero by less than the combined systematic uncertainty. For an intensity of 1×10^{-23} the difference is 0.23 % and for 1×10^{-24} it is 0.13 %. The results indicate the presence of line intensity dependent systematic errors of about 0.1 % in the intensity range 1×10^{-23} to 1×10^{-24} in at least one of the data sets. Relative errors among the four bands investigated in the present work were excluded based on number density fits of groups of measurements. Averages of number densities were formed for the different bands but individual number densities for each microwindow within each measurement as

Table 9
Comparison of experimental $d_{self/foreign,av,corr}$ and predicted $d_{self/foreign,av,pred}$. For symbols see Table 5.

	Ref	$d_{self/foreign,av}$/atm^{-1}	$d_{self/foreign,av,corr}$/atm^{-1}	$d_{self/foreign,av,pred}$/atm^{-1}
CO_2-CO_2, 294 K	Fig. 11 in this work	−0.00813	−0.0106	−0.0105
CO_2-CO_2, 212 K	Fig. 12 in this work	−0.0260	−0.0293	−0.0268
HCl-HCl, 293 K	Fig. 8 in [37]	−0.0262	−0.0324	−0.0127
HCl-air, 293 K	Fig. 4 in [38]	−0.00315	−0.00491	−0.00467
HCl-CO_2, 293 K	Fig. 4 in [38]	−0.00997	−0.0125	−0.0122
CO-N_2, 296 K	Fig. 2 in [28]	−0.000708	−0.00154	−0.000566

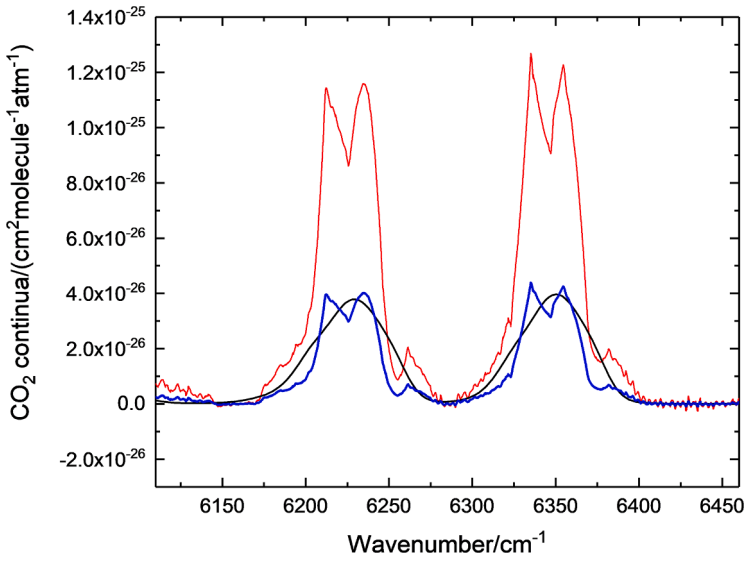

Fig. 15. Ambient temperature experimental CO_2 self- (red) and foreign- (blue) continua and MT_CKD foreign-continuum (black).

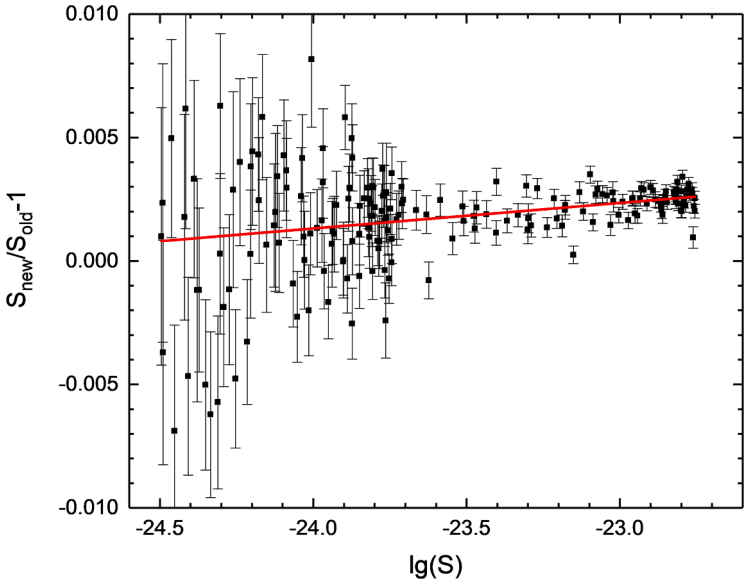

Fig. 16. Intensity ratio−1 of present work (new) and [8] (old) vs. logarithm of line intensity. 1σ combined statistical error bars are shown. The red line represents a linear fit in lg(S).

function of line intensity were, in contrast to the present work (see Fig. 2), not considered. The absence of significant slopes for most measurements in Fig. 2 is a clear indication of the absence of intensity-dependent systematic relative errors in the present work. In the old measurements, there were significant slopes present, which now may be interpreted as an indication of intensity-dependent systematic relative errors. In the old measurements, the maximum pressure was 80 mbar, thus instrumental line shape induced errors have a larger impact than in the present work with maximum pressures up to 1000 mbar. Furthermore, an offset error was detected later and not considered in [8]. During the analysis of [8] the intensity depletion was not known and thus not considered. In conclusion, an intensity-dependent systematic relative error in [8] is likely. The reason for such errors is linked to the error propagation of instrumental or line shape errors as function of optical depth, described in Section 5.5 “Relative errors and uncertainties” in [8]. In Table 10, intensity ratio averages for individual bands are listed, indicating that among the four bands the impact of the relative error is less than 0.05 %. The intensity ratios for the four bands together with the band-wise averages can be seen in Fig. 17. Note that the 30011 and 30014 bands are significantly weaker than the 30012 and 30013 bands (see Fig. 1 in [8]). A major difference in the analysis of this work is the introduction of the depletion parameter. The maximum pressure in [8] was 80 mbar. Note that the line intensities were calculated from 10, 30, and 80 mbar measurements. The d_{self} cover a range of about 0.6 %/atm, thus, for the old measurements the impact on relative line intensities within a band is at most 0.05 %. This small effect is not

Table 10
Averaged line intensity ratios from new, old [8], and HITRAN2020 data for 1.6 μm bands. 1σ in units of the last digit are given in parentheses.

Band	$S_{new}/S_{old}-1$	$S_{new}/S_{HITRAN2020}-1$
30011	0.00182(25)	0.00189(38)
30012	0.002261(86)	−0.003163(96)
30013	0.002468(79)	0.000990(87)
30014	0.00188(36)	0.00424(19)

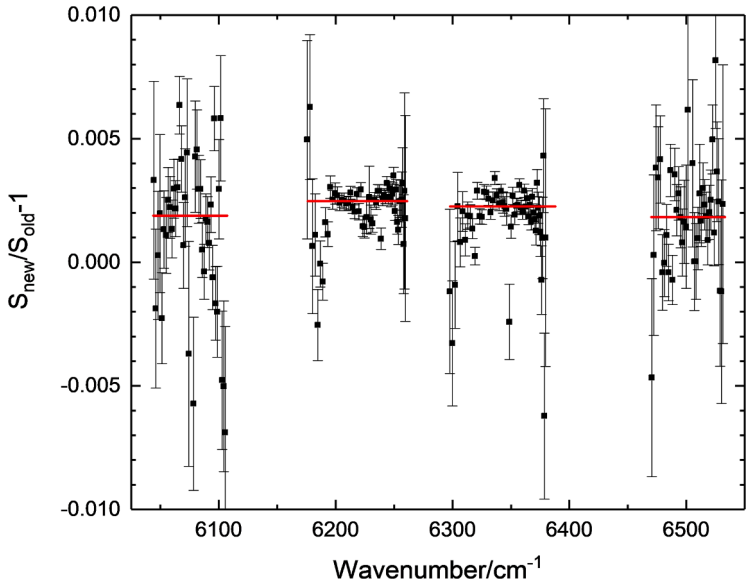

Fig. 17. Intensity ratio−1 of present work (new) and [8] (old) vs. wavenumber. 1σ combined statistical error bars are shown. From left to right: 30014, 30013, 30012, and 30011 bands. Red lines indicate weighted average intensity ratios for each band.

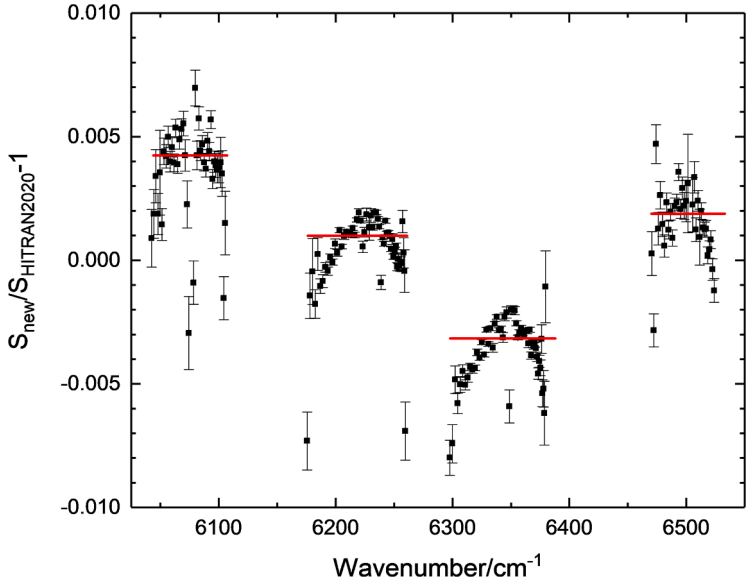

Fig. 18. Intensity ratio−1 of present work (new) and HITRAN2020 vs. wavenumber. 1σ statistical error bars of present work are shown. From left to right: 30014, 30013, 30012, and 30011 bands. Red lines indicate weighted average intensity ratios for each band.

visible in Fig. 17 since the impact of the intensity-dependent relative error is larger. In Fig. 18, new line intensities are compared to HITRAN2020 [19]. The average differences for the four bands range between −0.3 and +0.4 % and are listed in Table 10. The smaller statistical uncertainty in the present work allows a better comparison of the intensities within each band. There are systematic *m*-dependent differences up to 0.3 %. These differences are not visible in the comparison of the experimental data and are attributed to the *ab initio* calculations HITRAN2020 is based on.

6.3. Self-broadening

The self-broadening parameters of [8] and this work are compared in Fig. 19. On the average the agreement is better than 0.1 % for strong lines and 0.4 % for weak lines. The systematic uncertainty in [8] was 0.26 % and in the present work it is 0.09 %. For lines stronger than 3×10^{-25} the difference is within the combined systematic uncertainty.

7. Database

The spectroscopic database is based on HITRAN2020 with ca. 27,000 lines in the range 5970–6575 cm^{-1}. It is given in an extended HITRAN format and can be found together with the readme file and measurement database in Zenodo [43]. It is of similar format as the extended HITRAN version of [8], where the parameters determined in the present work were exchanged or, in case of parameters not present in [8], added. Parameters and uncertainties have been re-arranged for better readability. In case of line positions and pressure-induced shifts, only statistical uncertainties are given in the database, for all other parameters combined systematic uncertainties and statistical uncertainties are given separately. In case of line intensities statistical, combined systematic, and temperature-related standard uncertainties are given separately.

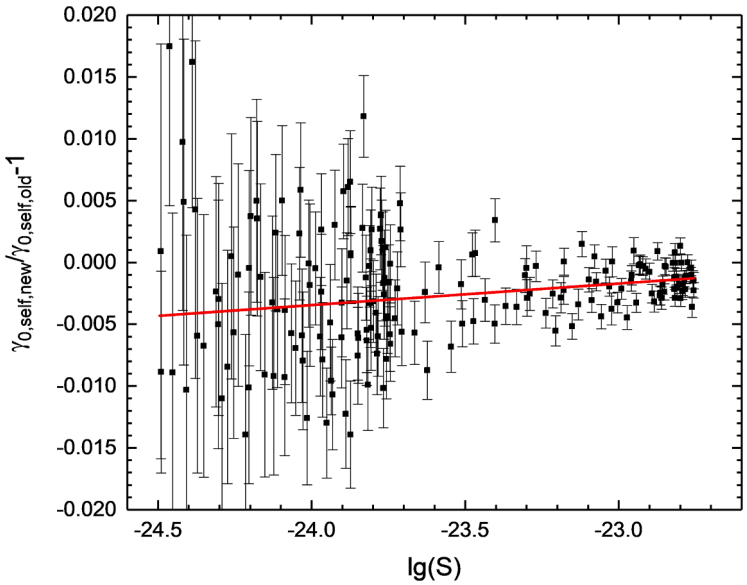

Fig. 19. Self-broadening parameter ratio−1 of present work (new) and [8] (old) vs. logarithm of line intensity. 1σ combined statistical error bars are shown. The red line represents a linear fit in lg(S).

Table 11
Number of lines for which a given parameter was fitted together with the threshold of statistical uncertainty below which a parameter was fitted.

Parameter	# of lines	Threshold of statistical uncertainty
σ_0	1178	0.005 cm^{-1}
S	1169	20 %
$d_{self,294K}$	202	0.004 atm^{-1}
$\gamma_{0,self}$	1193	10 %
$\gamma_{2,self}$	346	20 %
ν_{VC}	62	50 %
$Y_{self,294K}$	255	50 %
$\delta_{0,self}$	1198	0.01 cm^{-1}/atm
$\delta_{2,self}$	80	50 %
$d_{self,212K}$	194	0.005 atm^{-1}
n_{self}	632	0.2
$n_{\gamma 2,self}$	113	0.2
$Y_{self,212K}$	298	50 %
$T\delta_{0,self}$	234	2×10^{-5} cm^{-1}/atm

The isotopologue abundance of $^{13}C^{16}O_2$ (931 lines fitted) was considered in the line intensities as stated in [8]. The intensities of the less abundant isotopologues $^{12}C^{18}O^{16}O$ (120 lines fitted) and $^{12}C^{17}O^{16}O$ (118 lines fitted) should be regarded with care since no information on isotopologue abundance in the sample was available.

A summary of the number of lines for which a given parameter was fitted together with the threshold of statistical uncertainty below which a parameter was fitted is presented in Table 11. Line mixing and depletion are given for 294 K and 212 K.

Table 12 shows the summary of statistical and systematic/temperature-related standard uncertainties for the individual parameters. For line intensity and self-broadening, the statistical standard uncertainty is <0.1 % for the stronger lines. The weakest line intensity is about 6×10^{-27} $cm^{-1}cm^2molecule^{-1}$, the strongest 6×10^{-23} $cm^{-1}cm^2molecule^{-1}$.

The continua for 212 K and 294 K are also given, together with uncertainties [43].

When using the spectroscopic database together with the continua provided in this work, it is important to cut the line profiles at ±25 cm^{-1}. In order to use the database at other temperatures than 294 K and 212 K, the user may implement linear interpolation for line mixing, depletion, and continuum.

8. Conclusion

Fourier-transform measurements of pure CO_2 in the 1.6 μm region covering bands from ground state to 30011, 30012, 30013, and 30014 states at ambient temperature and 212 K with pressures up to 1 bar have been recorded. Line parameters have been retrieved by multispectrum fitting. An intensity correction parameter quantifying linear intensity dependence on pressure was introduced and fitted. From the fitted baseline polynomials, the self-continuum was determined for the 30012 and 30013 bands. The depleted intensity was found to be transferred to the continuum for both temperatures. The intensity in the continuum at 1 atm was about 1 % and 3 % of the total band intensities at ambient temperature and 212 K, respectively. An excellent agreement was found between the depleted/continuum intensity and the predicted depletion based on the second virial coefficient. Thus, the depletion/continuum is linked to an effective dimerization, which could be interpreted as quasi-bound dimer or free pairs alone. However, a contribution of a bound dimer in the continuum may be present, having a similar shape and about twice the intensity of the monomer band.

Table 12
Range of statistical standard uncertainties, combined systematical and temperature-related standard uncertainties.

	σ_0/cm^{-1}	S/%	$\gamma_{0,\sigma\varepsilon\lambda\phi}$/ %	$\gamma_{2,\sigma\varepsilon\lambda\phi}$/ %	$\delta_{0,\sigma\varepsilon\lambda\phi}/(cm^{-1}atm^{-1})$	$d_{self,294K}$	$d_{self,212K}$	n_{self}
Statistical (Type A)	1.6×10^{-6} – 3.8×10^{-3}	0.009 – 20	0.01 – 10	0.3 – 20	1.2×10^{-5} – 7×10^{-3}	1.3×10^{-4} – 3.5×10^{-3}	7×10^{-5} – 5×10^{-3}	3×10^{-4} – 0.2
Combined systematic (Type B)	1.7×10^{-6}	0.06	0.09	1	2×10^{-6}	8 %	2.30 %	0.03
T-related (Type B)		+0.25 – −0.08						

The continuum could be fitted from the depleted intensities as the sum of broad pressure-independent super-Lorentzian single line contributions with Lorentzian halfwidths linearly increasing with $|m|$, and line mixing linearly decreasing with m.

The present work gives more insight into the physical nature of continua. Quasi-bound dimers/free pairs may be the same as super-Lorentzian line wings caused by non-Markovian collisions contributing to the second virial coefficient.

Retrieval simulations for the CO_2 measurements planned with the future CO2M mission, similar to the OCO mission, were carried out to assess the impact of intensity depletion and continuum [21]. For TRO atmosphere, omitting the intensity depletion yields 0.2 % decreased CO_2 column for both, the 1.6 μm and 2 μm bands, while omitting both, depletion and continuum, results in an increase of the CO_2 column by 0.29 % and 1.5 % (0.35 % and 2.0 % for SAW atmosphere), respectively. Ignoring depletion and continuum yields 0.05 % and 0.47 % smaller CO_2 columns for tropical compared to subarctic winter atmosphere for the 1.6 μm and 2 μm bands, respectively. Furthermore, large residuals up to 1.1 % result in case of the 2 μm band. These results clearly exceed the allowed error budget, showing the importance of depletion and continuum for the satellite data processing. The impact of the continuum is larger than that of the depletion, especially for the 2 μm band. Considering only the depletion in the radiative transfer would lead to worse results in the atmospheric retrieval than ignoring both depletion and continuum.

When compared to our previous work [8], several instrumental improvements have been achieved to reduce the systematic uncertainties of line intensities to well below 0.1 %. The line model was improved by adding d_{self}. The new line intensities are larger by 0.23 % for an intensity of 1×10^{-23}, and 0.13 % for an intensity of 1×10^{-24}. This difference is within the combined uncertainties of previous and present work. A new spectroscopic database together with a measurement database was produced and published on ZENODO [43].

The best approach to obtain a spectroscopic database containing d_{self} and continuum is to determine both from the same measurements. An error in the line model would be covered in the continuum as long as residuals of the fit are noise. In the atmospheric retrieval, it is advantageous to use the line parameters and continuum from the same source to assure that line parameters and continuum are consistent.

The essence of the present work is that we show for the first time that an in-band continuum can be the result of a line model deficit, having a pressure-independent broad super-Lorentzian line profile, scaling with the pressure squared. The regular line modelling shows PDIC but the sum of the integrated line spectrum and the continuum over the band does not depend on pressure. The average PDIC/continuum area agrees with the average PDIC predicted from the second virial coefficient.

An open issue is why the CIA of the Fermi dyad and triad shows CO_2 dimer structure while the CIA of $\nu_2+\nu_3$ and the results of the present work do not. It would be interesting to determine continua for the ν_2 and/or $3\nu_2$ and to see whether the bound dimer structure is present. For the ν_2 the dipole moment change with vibration is perpendicular to that of the ν_3.

In future, similar investigations for other molecules and for gas mixtures are needed to show whether the findings for CO_2 are generic. The results may help to predict the average PDIC/continuum area from the second virial coefficient. In case the measurement of either PDIC or continuum is difficult, estimates based on the more accessible quantity can be made. The theory of continua as well as the database may be improved using the findings of the present work.

CRediT authorship contribution statement

M. Birk: Writing – review & editing, Writing – original draft, Visualization, Supervision, Software, Project administration, Methodology, Investigation, Funding acquisition, Formal analysis, Conceptualization. **C. Röske:** Writing – review & editing, Software, Investigation. **G. Wagner:** Writing – review & editing, Writing – original draft, Visualization, Software, Methodology, Investigation, Funding acquisition, Formal analysis.

Declaration of competing interest

The authors declare that they have no known competing financial interests or personal relationships that could have appeared to influence the work reported in this paper.

Data availability

Measurement data and databases are available on ZENODO.

Acknowledgments

The authors like to thank Ha Tran and Jean-Michel Hartmann for their support in writing this paper. Furthermore, we want to thank Ha Tran for calculation of CO_2 spectra with full relaxation matrix. The authors want to thank Mikhail Tretyakov for fruitful discussions on the present work and the nature of CIA. The work was partly funded by the European Space Agency under Contract No. 4000132228/20/I-NS, 2020.

References

[1] Anderson GP, Chetwynd JH, Clough SA, Shettle EP, Kneizys FX. AFGL atmospheric constituent profiles (0-120km), AFGL-TR-86-011. Hanscom AFB, MA: Air Force Geophysics Laboratory; 1986. p. 01731.
[2] Azentrischer Faktor – Wikipedia. https://de.wikipedia.org/wiki/Azentrischer_Faktor.
[3] Baranov YI, Fraser GT, Lafferty WJ, Vigasin AA. Collision-induced absorption in the CO_2 Fermi triad for temperatures from 211 K to 296 K (editors). In: Camy-Peyret C, Vigasin AA, editors. Weakly Interacting Molecular Pairs: Unconventional Absorbers of Radiation in the atmosphere. Dordrecht: Kluwer Academic Publishers; 2003. p. 149–58.
[4] Baranov YI. Collision-induced absorption in the region of the $\nu_2 + \nu_3$ band of carbon dioxide. J Molec Spectrosc 2018;345:11–6. https://doi.org/10.1016/j.jms.2017.11.005.
[5] Bielska K. Subpromille measurements and calculations of CO (3–0) overtone line intensities. Phys Rev Let 2022;129:043002. https://doi.org/10.1103/PhysRevLett.129.043002.
[6] Birk M, Wagner G. Temperature-dependent air broadening of water in the 1250–1750 cm^{-1} range. J Quant Spectrosc Radiat Transfer 2012;113:889–928. https://doi.org/10.1016/j.jqsrt.2011.12.013.
[7] Birk M, Wagner G, Loos J, Shine KP. 3 μm Water vapor self- and foreign-continuum: new method for determination and new insights into the self-continuum. J Quant Spectrosc Radiat Transfer 2020;253:107134. https://doi.org/10.1016/j.jqsrt.2020.107134.
[8] Birk M, Röske C, Wagner G. High accuracy CO_2 fourier transform measurements in the range 6000–7000 cm^{-1}. J Quant Spectrosc Radiat Transfer 2021;272:107791. https://doi.org/10.1016/j.jqsrt.2021.107791.
[9] M. Birk, G. Wagner, C. Röske, Fourier-transform intensity measurements with 0.1% accuracy. ASA - HITRAN 2022, 24–26. Aug. 2022, Reims, France.
[10] Bock S, Bich E, Vogel E. A new intermolecular potential energy surface for carbon dioxide from ab initio calculations. Chem Phys 2000;257:147. https://doi.org/10.1016/S0301-0104(00)00161-0.
[11] Boulet C, Flaud P-M, Hartmann JM. Infrared line collisional parameters of HCl in Argon, beyond the impact approximation: measurements and classical path calculations. J Chem Phys 2014;120:11053. https://doi.org/10.1063/1.1714794.
[12] Brugge HB, Hwang C-A, Rogers WJ, Holste JC, Hall KR, Lemming W, Esper GJ, Marsh KN, Gammon BE. Experimental cross virial coefficients for binary mixtures of carbon dioxide with nitrogen, methan and ethane at 300 and 320 K. Physica A 1989;156:382–416. https://doi.org/10.1016/0378-4371(89)90131-3.
[13] S.A. Clough F.X. Kneizys, R. Davies, R. Gamache, R. Tipping, Theoretical Line Shape for H2O Vapor: application to the Continuum, in "Atmospheric Water Vapor", Proceedings of the International Workshop on Atmospheric Water Vapor, Vail, Colorado, September 11-13, 1979, editors A. Deepak, T.D. Wilkerson, L.H. Ruhnke.
[14] Cole R, Tran H, Hoghooghi N, Rieker G. Temperature-dependent CO_2 line mixing models using dual frequency comb absorption and phase spectroscopy up to 25 bar and 1000 K. J Quant Spectrosc Radiat Transfer 2023;297:108488. https://doi.org/10.1016/j.jqsrt.2023.108488.
[15] Cottrell TL, Hamilton RA, Taubinger RP. The second virial coefficients of gases and mixtures, part 2.-mixtures of carbon dioxide with nitrogen, oxygen, carbon monoxide, argon and hydrogen. Trans Faraday Soc 1956;52:1310–2. https://doi.org/10.1039/TF9565201310.

[16] Dadson RS, Evans EJ, King JH. The second virial coefficient of carbon dioxide. Proc Phys Soc 1967;92:1115. https://doi.org/10.1088/0370-1328/92/4/337.
[17] Elliott JR. Appendix B. Lennard-Jones Potentials as Determined from Viscosity Data, Properties of Gases and Liquids. et al.. 6th Edition. McGraw-Hill Education; 2023.
[18] Fleurbaey H, Yi H, Adkins EM, Fleisher AJ, Hodges JT. Cavity ring-down spectroscopy of CO_2 near $\lambda = 2.06$ μm: accurate transition intensities for the Orbiting Carbon Observatory-2 (OCO-2) "strong band. J Quant Spectrosc Radiat Transfer 2020;252:107104. https://doi.org/10.1016/j.jqsrt.2020.107104.
[19] Gordon IE. The HITRAN2020 molecular spectroscopic database. J Quant Spectrosc Radiat Transfer 2022;277:107949. https://doi.org/10.1016/j.jqsrt.2021.107949.
[20] Hase F, Blumenstock T, Paton-Walsh C. Analysis of the Instrumental line shape of high-resolution fourier transform IR spectrometers with gas cell measurements and new retrieval software. Appl Opt 1999;38:3417–22. https://doi.org/10.1364/AO.38.003417.
[21] Improved Spectroscopy for Carbon Dioxide, Oxygen, and Water Vapour Satellite Measurements (ISOGG), ESA Contract No. 4000132228/20/I-NS, 2020.
[22] Kouzov AP, Tokhadze KG, Utkina SS. Buffer-gas effect on the rotovibrational line intensity distribution: analysis of possible mechanisms. Eur Phys J D 2000;12:153–9. https://doi.org/10.1007/s100530070052.
[23] Kouzov AP, Sokolov AV, Filippov NN. Non-Markovian approach to pressure broadening of isolated lines in spectra of light rotators. J Quant Spectrosc Rad Transfer 2022;278:108043. https://doi.org/10.1016/j.jqsrt.2021.108043.
[24] Long DA, Reed ZD, Fleisher AJ, Mendonca J, Roche S, Hodges JT. High-accuracy near-infrared carbon dioxide intensity measurements to support remote sensing. Geophys Res Lett 2020;47:e2019GL086344. https://doi.org/10.1029/2019GL086344.
[25] Mlawer EJ, Payne VH, Moncet JL, Delamere JS, Alvarado MJ, Tobin DC. Development and recent evaluation of the MT_CKD model of continuum absorption. Phil Trans R Soc A 2012;370:2520–56. https://doi.org/10.1098/rsta.2011.0295.
[26] Ngo NH, Lisak D, Tran H, Hartmann JM. An isolated line-shape model to go beyond the Voigt profile in spectroscopic databases and radiative transfer codes. J Quant Spectrosc Radiat Transf 2013;129:89–100. https://doi.org/10.1016/j.jqsrt.2013.05.034. Associated Erratum: J Quant Spectrosc Radiat Transfer 2014;134:105.
[27] Ptashnik IV, Klimeshina TE, Solodov AA, Vigasin AA. Spectral composition of the water vapour self-continuum absorption within 2.7 and 6.25 μm bands. J Quant Spectrosc Radiat Transfer 2019;228:97–105. https://doi.org/10.1016/j.jqsrt.2019.02.024.
[28] Reed ZD, Tran H, Ngo HN, Hartmann JM, Hodges JT. Effect of non-markovian collisions on measured integrated line shapes of CO. Phys Rev Lett 2023;130:143001. https://doi.org/10.1103/PhysRevLett.130.143001.
[29] Rosenkranz PW. Shape of the 5 mm oxygen band in the atmosphere. IEEE Trans Antennas Propag 1975;AP-23:498–506. https://doi.org/10.1109/TAP.1975.1141119.
[30] Schramm B, Leuchs U. Zweite Virialkoeffizienten von HCl, DCl und Ar - HCl-Mischungen. Ber Bunsenges Phys Chem 1979;83:847. https://doi.org/10.1002/bbpc.19790830815.
[31] Scientific Exploitation of Operational Missions - Improved Atmospheric Spectroscopy Databases (SEOM-IAS), ESA Contract No 4000110254/14/I-BG, 2014.
[32] Serov EA, Odintsova TA, Tretyakov MYu, Semenov VE. On the origin of the water vapour continuum absorption within rotational and fundamental vibrational bands. J Quant Spectrosc Radiat Transfer 2017;193:1–12. https://doi.org/10.1016/j.jqsrt.2017.02.011.
[33] Shine KP, Ptashnik IV, Rädel G. The water vapour continuum: brief history and recent developments. Surv Geophys 2012;33:535–55. https://doi.org/10.1007/s10712-011-9170-y.
[34] Soave-Redlich-Kwong-Zustandsgleichung – Wikipedia. https://de.wikipedia.org/wiki/Soave-Redlich-Kwong-Zustandsgleichung.
[35] Tran H, Boulet C, Stefani S, Snels M, Piccioni G. Measurements and modelling of high pressure pure CO2 spectra from 750 to 8500 cm^{-1}. I—central and wing regions of the allowed vibrational bands. J Quant Spectrosc Radiat Transfer 2011;112(6):925–36. https://doi.org/10.1016/j.jqsrt.2010.11.021.
[36] Tran H, Li G, Ebert V, Hartmann JM. Super- and sub-Lorentzian effects in the Ar-broadened line wings of HCl gas. J Chem Phys 2017;146:194305. https://doi.org/10.1063/1.4983397.
[37] Tran H, Li G, Ngo NH, Ebert V. Pressure dependence of the measured line intensity and super-Lorentzian effects in the absorption spectra of pure HCl. Phys Chem Chem Phys 2023;25:10343–52. https://doi.org/10.1039/D2CP04892B.
[38] Tran H, Li G, Ngo NH, Ebert V. Non-impact effects in the absorption spectra of HCl diluted in CO_2, air, and He: measurements and predictions. J Chem Phys 2023;158:184301. https://doi.org/10.1063/5.0147916.
[39] Vigasin AA. Bound, metastable and free states of bimolecular complexes. Infrared Phys 1991;32:461–70. https://doi.org/10.1016/0020-0891(91)90135-3.
[40] Vigasin AA, Baranov YI, Chlenova GV. Temperature variations of the interaction induced absorption of CO_2 in the ν_1, $2\nu_2$ region: FTIR measurements and dimer contribution. J Molec Spectrosc 2002;213:51–6. https://doi.org/10.1006/jmsp.2002.8529.
[41] Vigasin AA, Ivanov SV. The effect of perturbing gas density on the intensity distribution in rovibrational absorption bands. Chem Phys 2006;325:404–10. https://doi.org/10.1016/j.chemphys.2006.01.011.
[42] Wilzewski J, Birk M, Loos J, Wagner G. Temperature-dependence laws of absorption line shape parameters of the CO_2 N_3 BAND. J Quant Spectrosc Radiat Transfer 2018;206:296–305. https://doi.org/10.1016/j.jqsrt.2017.11.021.
[43] ZENODO https://doi.org/10.5281/zenodo.10727028.